Monthly Notices
of the
ROYAL ASTRONOMICAL SOCIETY

MNRAS **502,** 601–620 (2021)
Advance Access publication 2021 January 8

doi:10.1093/mnras/staa4020

The VVV near-IR galaxy catalogue beyond the Galactic disc

Laura D. Baravalle,[1]★ María Victoria Alonso,[1,2]★ Dante Minniti,[3,4,5] José Luis Nilo Castellón,[6,7] Mario Soto,[8] Carlos Valotto,[1,2] Carolina Villalón,[1] Darío Graña,[1] Eduardo B. Amôres[9] and Fernanda Milla Castro[6]

[1]*Instituto de Astronomía Teórica y Experimental (IATE, CONICET-UNC), Laprida 854, Córdoba, X5000BGR, Argentina*
[2]*Observatorio Astronómico de Córdoba, Universidad Nacional de Córdoba, Córdoba, X5000BGR, Argentina*
[3]*Departamento de Física, Facultad de Ciencias Exactas, Universidad Andrés Bello, Av. Fernandez Concha 700, Las Condes, Santiago, Chile*
[4]*Instituto Milenio de Astrofísica, Santiago, 7500912, Chile*
[5]*Vatican Observatory, V-00120 Vatican City State, Italy*
[6]*Departamento de Física y Astronomía, Facultad de Ciencias, Universidad de La Serena, Av. Juan Cisternas 1200 Norte, La Serena, Chile*
[7]*Instituto de Investigación Multidisciplinario en Ciencia y Tecnología, Universidad de La Serena. Av. Juan Cisternas 1400, La Serena, Chile*
[8]*Instituto de Astronomía y Ciencias Planetarias, Universidad de Atacama, Copayapu 485, Copiapó, Chile*
[9]*Departamento de Física, Universidade Estadual de Feira de Santana (UEFS), Av. Trans. S/N, CEP 44036-900 Feira de Santana, BA, Brazil*

Accepted 2020 December 22. Received 2020 December 22; in original form 2020 June 2

ABSTRACT

Knowledge about the large-scale distribution of galaxies is far from complete in the Zone of Avoidance (ZoA), which is mostly due to high interstellar extinction and to source confusion at lower Galactic latitudes. Past near-infrared (NIR) surveys, such as the Two Micron All Sky Survey (2MASS), have shown the power of probing large-scale structure at these latitudes. Our aim is to map the galaxy distribution across the Southern Galactic plane using the VISTA Variables in the Vía Láctea Survey (VVV), which reach 2–4 mag deeper than 2MASS. We used SExtractor+PSFEx to identify extended objects and to measure their sizes, the light concentration index, magnitudes, and colours. Morphological and colour constraints and visual inspection were used to confirm galaxies. We present the resulting VVV NIR Galaxy Catalogue (VVV NIRGC) of 5563 visually confirmed galaxies, of which only 45 were previously known. This is the largest catalogue of galaxies towards the Galactic plane, with 99 per cent of these galaxies being new discoveries. We found that the galaxy density distribution closely resembled the distribution of low interstellar extinction of the existing NIR maps. We also present a description of the 185 2MASS extended sources observed in the region, of which 16 per cent of these objects had no previous description, which we have now classified. We conclude that interstellar extinction and stellar density are the main limitations for the detection of background galaxies in the ZoA. The VVV NIRGC is a new data set providing information for extragalactic studies in the Galactic plane.

Key words: catalogues – surveys – galaxies: photometry – infrared: galaxies.

1 INTRODUCTION

The identification of galaxies behind the Milky Way (MW) is a difficult task, due to the obscuring effects of both dust and stars, and also the high stellar crowding at low Galactic latitudes (Kraan-Korteweg & Lahav 2000). The hidden galaxies can contribute to the identification of large-scale structures beyond our Galaxy (Huchra et al. 2012; Macri et al. 2019), as these allow us to obtain complete luminosity, mass, and density distributions that can be tested against the models of galaxy and structure formation (Peebles 1980; Klypin et al. 1993).

At optical wavelengths, systematic searches for galaxies towards the obscured regions in our Galaxy have been performed to reduce the effects of the Zone of Avoidance (ZoA). Kraan-Korteweg & Woudt (1999), Kraan-Korteweg (2000), and Woudt & Kraan-Korteweg (2001) presented the first deep optical search for galaxies using the object's diameter for the selection of candidates behind the MW, with these authors identifying overdensities and filaments of galaxies that might be related to possible extragalactic large-scale structures.

The use of near-infrared (NIR) surveys minimizes the effects of foreground extinction in the ZoA in comparison with optical passbands. The Two Micron All Sky Survey (2MASS; Skrutskie et al. 2006) produced images in the J, H, and K_s NIR passbands, while Jarrett et al. (2000a) developed an algorithm to detect and characterize extended sources in the 2MASS catalogue. The procedure to separate point sources from extended sources includes tracking the point spread function (PSF), image background removal, photometry, and object classification, using a decision tree technique which takes into account the radial shape, surface brightness, and symmetry parameters of the sources. Near the Galactic plane ($|b| < 3^\circ$), the extended sources are dominated by galaxies, Galactic H II regions and large low surface brightness nebulae, stellar clusters, and multiple stars. The main science products of this survey are the Point Source Catalog (PSC), consisting of over 500 million stars and galaxies, and the Extended Source Catalog (2MASX) with 1.6 million resolved sources complete to $K_s = 13.5$ mag, and covering more than 99 per cent of the sky. Jarrett et al. (2000b) reported the

★ E-mail: lbaravalle@unc.edu.ar (LDB); m.v.alonso@unc.edu.ar (MVA)

detection and spectroscopic confirmation of nearby galaxies hidden behind the MW data in the ZoA. Later, Schröder et al. (2007) performed a visual search for galaxies based on the Deep Near Infrared Survey (Epchtein et al. 1997) and compared these results with objects in common with 2MASX. These authors presented a catalogue of 122 galaxies and possible galaxy candidates, including morphological types estimated from the galaxy appearance in the *I*, *J*, and *K* passbands, and total magnitudes and errors derived using the MAG_AUTO magnitudes from SExtractor (Bertin & Arnouts 1996). More recently, Schröder, an Driel & Kraan-Korteweg (2019a) presented a homogeneous bright galaxy catalogue of 3763 objects based on the 2MASX survey at latitudes lower than 10°, with the main goal of obtaining the Tully–Fisher (TF) relation to this whole-sky sample.

The 2MASS Redshift Survey (2MRS, Huchra et al. 2005, 2012; Macri et al. 2019) provides redshifts for the 45 640 brightest 2MASS galaxies (extinction-corrected $K_s < 11.75$ mag) in the regions defined as $|b| \geq 5°$ for $30° < l < 330°$ and $|b| \geq 8°$ for other l values. The radial velocities of this survey might be able to contribute to studies of large-scale structures and cosmic flows in this important region of the hidden sky. In this sense, the 2MASS Tully–Fisher survey (2MTF, Masters, Springob & Huchra 2008; Howlett et al. 2017) aims to measure distances of all bright spirals using the TF relation. Finally, Lambert et al. (2020) applied to this catalogue a modification to the traditional friends-of-friends algorithm (Huchra & Geller 1982), and found new group candidates that might help to define new large-scale structures in the ZoA.

Staveley-Smith et al. (2016) presented the deep H I survey (HI-ZOA) in the southern ZoA covering the region of $212° < l < 36°$ and $|b| < 5°$. These H I surveys allow the study of sources in this region because they suffer minimal foreground extinction or source confusion when compared with optical and NIR surveys. These surveys are complementary, as NIR selection mainly favours the detection of early-type galaxies, while H I surveys the late-types. Sorce et al. (2017) predicted structures towards the ZoA by performing simulations that yielded a probability distribution of galaxies. They then compared their results with a dozen known galaxy clusters, including the presence of the more distant Vela super-cluster (Kraan-Korteweg et al. 2017), and found a remarkable agreement. Finally, Schröder et al. (2019b) presented detections of 170 galaxies in the northern ZoA at $|b| < 6°$, of which a third of these had no previous H I observations.

Recent NIR surveys have increased the capacity for detecting extragalactic sources in the ZoA, as shown by Williams, Kraan-Korteweg & Woudt (2014), who presented a photometric catalogue of 548 HIZOA galaxies that reach 2 mag deeper than 2MASS in this region. The NIR properties include ellipticities, position angles, isophotal, and extrapolated total magnitudes in the three *J*, *H*, and K_s NIR passbands. Said et al. (2016) presented a deep NIR catalogue of 915 galaxies from the HIZOA, that includes ellipticities in the *J* passband and isophotal magnitudes at $K_s = 20$ mag arcsec^{-2} in the *J*, *H,* and K_s passbands. Their main goal was to obtain accurate NIR photometric parameters for the NIR TF analysis. This work is an extension of Williams et al. (2014) with the addition of new observations. The photometric and spectroscopic surveys are primordial to understand the large-scale structure in this complicated region due to the presence of the MW. All the surveys involving NIR data, including 2MASX, 2MRS, and 2MTF, and the 'blind' H I data, such as HIZOA, are complementary. Important structures in the local Universe such as the Great Attractor (for a review of its size and location see Mutabazi et al. 2014) and Norma cluster (Kraan-Korteweg et al. 1996) are found in these regions. The combination of all surveys will allow peculiar velocities to be determined, in order to obtain a better understanding of the local dynamics, the cosmic flow fields and the underlying density field (Kraan-Korteweg et al. 2018).

The VISTA (Visible and Infrared Survey Telescope for Astronomy) Variables in the Vía Láctea (VVV, Minniti et al. 2010) is an NIR variability survey of the entire MW Bulge and a large portion of the Southern Galactic disc, with the main scientific goal being to gain more insight into the inner MW's origin, structure, and evolution. This survey has detected objects that are hidden behind Galactic high extinction regions, and these discoveries include variable stars, brown dwarfs (Beamín et al. 2013), new stellar open clusters (Borissova et al. 2011, 2014; Barbá et al. 2015), and new globular clusters (Minniti et al. 2011, 2017).

In addition to studies of Galactic structure, the VVV survey also offers an excellent opportunity to study extragalactic sources behind the MW, such as background galaxies, active galaxies including quasars and blazars, and groups and clusters of galaxies. In this sense, Amôres et al. (2012) identified 214 galaxy candidates in the d003 tile of the VVV survey ($l = 298.356°$ and $b = -1.650°$) behind the Galactic disc, by means of visual inspection and a comparison of their sizes and colours with field stars. Coldwell et al. (2014) confirmed the existence of the X-ray-detected galaxy cluster Suzaku J1759−3450 (Mori et al. 2013) at $z = 0.13$ in the b261 tile ($l = 356.597°$ and $b = -5.321°$), with the photometry of the sources being obtained using SExtractor (Bertin & Arnouts 1996).

Baravalle et al. (2018) was our first galaxy search study in the reddened and crowded fields located at low Galactic latitudes. We presented a photometric method based on SExtractor+PSFEx (Bertin & Arnouts 1996; Bertin 2011) to identify and characterize extragalactic sources behind the MW disc. The method was tested in the d010 ($l = 308.569°$ and $b = -1.649°$) and d115 ($l = 295.438°$ and $b = 1.627°$) tiles, and revealed 530 new galaxy candidates. Baravalle et al. (2019) presented the first confirmed galaxy cluster VVV-J144321.06−611753.9 at $z = 0.234$ in the VVV d015 tile ($l = 315.836°$ and $b = -1.650°$). The photometry was performed with SExtractor+PSFEx using the Baravalle et al. (2018) procedure, and the selection was based on the cluster red sequence in the colour–magnitude diagrams (Gladders & Yee 2000).

More recently, Saito et al. (2019) reported that VVV-WIT-04, an NIR variable source, has an extragalactic origin and might be the counterpart of the radio source PMN J1515−5559. Pichel et al. (2020) presented the NIR and mid-IR (MIR) properties of four known blazars located in the VVV regions, which have very different NIR properties in the colour–magnitude and colour–colour diagrams compared with stellar or extragalactic sources, and also exhibit a significant variability in the K_s light curves.

Baravalle et al. (2018, 2019) optimized the photometric procedure in order to identify and characterize extended sources. Here, we used the VVV NIR images across the Southern Galactic disc and we present the photometric catalogue of galaxies in the ZoA. This catalogue will allow the community to pursue a number of different scientific projects such as mapping the total extinction across the Galactic plane, and to recognize clear NIR windows of low interstellar extinction (Minniti et al. 2018; Saito et al. 2020). Other related projects involve associate galaxy hosts for transient sources, including supernovae, gamma-ray bursts, and gravitational wave events, to search for hidden nearby galaxies at low Galactic latitudes and to identify candidates for compact groups and clusters of galaxies. The paper is organized as follows: Section 2 presents the VVV NIR data, including principally the methodology to identify extragalactic sources and confirmed galaxies, as well as the comparison with other NIR surveys and the correlation with MIR data.

Section 3 presents the VVV NIR Galaxy Catalogue (VVV NIRGC) in the Southern Galactic disc of the survey and the galaxy distribution map. Section 4 includes the principal conclusions and final remarks.

2 THE VVV SURVEY

The NIR observations allow the study of regions at the lower Galactic latitudes, where interstellar extinction is severe. This wavelength regime is less affected by foreground extinction than the optical one. It is also sensitive to early-type galaxies, groups, and galaxy clusters, which should be less confused with Galactic objects such as young stellar objects (YSO) and cool cirrus sources (Schröder et al. 2007).

The VVV survey is an NIR variability public survey of the Galactic bulge ($10^\circ < l < 350^\circ$ and $-10^\circ < b < +5^\circ$) and an adjacent section of the mid-plane ($295^\circ < l < 350^\circ$ and $-2^\circ < b < +2^\circ$) (Minniti et al. 2010). The survey was carried out using the VISTA 4-m telescope at ESO, which is equipped with a wide-field NIR camera (VIRCAM, Dalton et al. 2006) with a pixel scale of 0.34 arcsec pixel^{-1}.

The VVV tiles are produced by six single pointing observations with a total field of view of 1.64 deg^2 in the Z (0.87 μm), Y (1.02 μm), J (1.25 μm), H (1.64 μm), and K_s (2.14 μm) passbands (Saito et al. 2010). The VVV images were taken under varying observing conditions, although in general this effect would be minimal because we use images with seeing < 0.9 arcsec in the K_s passbands. The background sky level varies from image to image, and the source density changes with position across the MW disc, depending on the line of sight. The survey area is fully covered by 348 tiles in the MW, of which 196 are in the bulge and 152 in the disc regions. In this work, we focused our efforts on the disc parts of 220 deg^2 covered by the survey. The images from the Project Programme 179.B-2002 were downloaded from the Cambridge Astronomical Survey Unit[1] (CASU, Emerson, McPherson & Sutherland 2006) with the observing status 'Completed', with the same exposure time and the smallest observed seeing.

In the future, the VVV eXtended Survey (VVVX) will triple the areal coverage of the original VVV survey following the same observational strategy. This extended survey, aimed for completion in late 2021, will provide J, H, and K_s astrometric and photometric catalogues reaching similar magnitudes for the extended area, as well as variability information for the K_s passband. The galaxies found in these regions would connect the VVV galaxy distribution with other surveys at higher Galactic latitudes.

2.1 The methodology

The algorithm to detect and characterize extragalactic sources using SExtractor (Bertin & Arnouts 1996) and PSFEX (Bertin 2011) has been extensively described in Baravalle et al. (2018). Briefly, SExtractor performs the photometry in the Z, Y, J, H, and K_s VVV images and creates catalogues for each passband. PSFEX takes these catalogues and creates the best PSF model by looking for well-defined point sources. Finally, SExtractor+PSFEx applies the PSF model to each source to obtain the astrometric, photometric, and morphological properties.

We applied the custom-built pipeline to the 152 tiles of the Galactic disc region using only the J, H, and K_s images, as most of the galaxies have no light contributions in the Z and Y passbands. All detected sources in these passbands were cross-matched taking the K_s passband as a reference, using the maximum object separation of 1 arcsec.

[1] http://casu.ast.cam.ac.uk/vistasp/imgquery/search

In order to discriminate point sources from extended objects, we used magnitudes, the stellar index *CLASS_STAR*, the SPREAD_MODEL (Φ) parameter, the radius that contains 50 per cent of the total flux of an object ($R_{1/2}$), and the concentration index (C, Conselice, Bershady & Jangren 2000) from the K_s detections. The extended sources have to satisfy the morphological criteria: *CLASS_STAR* < 0.3; $\Phi > 0.002$; $1.0 < R_{1/2} < 5.0$ arcsec and $2.1 < C < 5$ (Baravalle et al. 2018).

SExtractor performs a clean procedure for any source inside the adaptive aperture, in which the fluxes are integrated by applying a mirroring between one side of the ellipse and the other. Also, the flux is defined by taking into account the threshold that separates the source from the background. The stellar density at lower Galactic latitudes makes it difficult to separate close objects degrading this process, and as this makes the adaptive apertures smaller, the magnitudes are underestimated. In order to minimize this effect, the cases with extreme contamination were not included in this study, which in fact represent a very small percentage of our total sample. The SExtractor photometry allowed us to obtain total magnitude (MAG_AUTO) estimates using the Kron (1980) magnitudes, which represent approximately 94 per cent of the total flux (Bertin & Arnouts 1996). SExtractor+PSFEx provided us with the PSF-fitting magnitudes (MAG_PSF), using the PSF model mentioned above, and also the circular aperture magnitudes obtained within a fixed aperture of 2 arcsec diameter to avoid strong stellar contamination. The $(J - K_s)$, $(J - H)$, and $(H - K_s)$ colours were then derived from these aperture magnitudes.

2.1.1 *Interstellar extinction and stellar density*

The extinction at lower Galactic latitudes is high in some parts of the MW. Schlegel, Finkbeiner & Davis (1998) derived extinction maps from the 100 μm dust emission by DIRBE/IRAS, which were re-calibrated by Schlafly & Finkbeiner (2011). At $|b| < 5^\circ$, the presence of contaminating sources was not removed and the reddening reported should be taken with caution (Arce & Goodman 1999; Amôres & Lépine 2005, 2007; Gonzalez et al. 2012; Soto et al. 2013, 2019). Nagayama et al. (2004) studied the distribution of galaxies at low Galactic latitudes ($b \sim 1.7^\circ$), and by using a stellar colour-excess technique these authors found a systematic underestimation of $A_K \sim 0.4$ mag in the map of Schlegel et al. (1998). However, despite these concerns, the maps are still widely used to characterize the foreground extinction in studies of the distribution of galaxies in the ZoA. In particular, the work of Schröder et al. (2007, 2019a) and van Driel et al. (2009) have used the Schlegel et al. (1998) maps to obtain the extinction-corrected magnitudes, and found them to be consistent with the 2MRS and 2MTF surveys. Our magnitudes were corrected by interstellar extinction along the line of sight, using the maps of Schlafly & Finkbeiner (2011) and the VVV NIR relative extinction coefficients of Catelan et al. (2011): $A_J = 0.280\,A_V$, $A_H = 0.184\,A_V$, and $A_{Ks} = 0.118\,A_V$. These corrected magnitudes and colours are represented by J°, H°, and K_s° and the colours $(J - K_s)^\circ$ and $(H - K_s)^\circ$ throughout this work.

2.1.2 *False detections and duplicate objects*

In order to minimize false detections, we also considered colour cuts: $0.5 < (J - K_s)^\circ < 2.0$ mag, $0.0 < (J - H)^\circ < 1.0$ mag, $0.0 < (H - K_s)^\circ < 2.0$ mag, and $(J - H)^\circ + 0.9\,(H - K_s)^\circ > 0.44$ mag following Baravalle et al. (2018). These cuts provide a good compromise between avoiding the loss of interesting objects and the inclusion of spurious ones, and these are similar to those used in Jarrett et al.

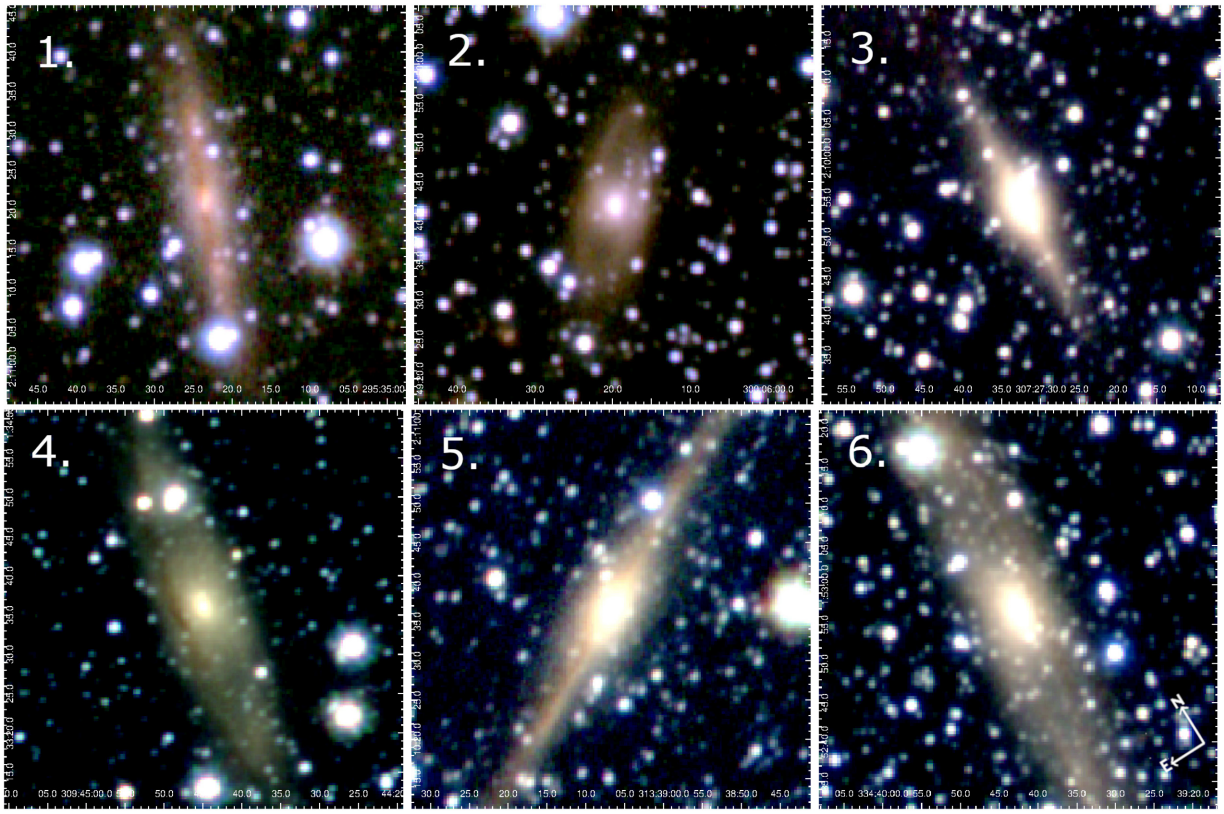

Figure 1. The VVV colour composed images of galaxies with strong stellar contamination. The panels show the sources: (1) J11523245−5950248, (2) J12280968−6054558, (3) J13281021−6022580, (4) J13471848−6034133, (5) J14155209−5855348, and (6) J16174633−4751584.

(2000a, b) and Amôres et al. (2012). This process classifies these objects as extragalactic candidates, and the final visual inspection allows us to confirm the galaxies. This inspection was performed by four of the authors of the present study for all the candidates by looking at the images in the five passbands of the VVV survey using the VISTA Science Archive (VSA[2]). When any doubts, discrepancies and/or comments arose, we searched for false three-colour images generated from the J, H, and K_s passbands. The combined colour and the extended nature allowed us to distinguish better the true galaxies from false ones. Some objects were also found with important stellar contamination, with Fig. 1 showing examples of the largest galaxies detected with strong stellar contamination. These objects were also observed by the 2MASX survey. In our first investigation (Baravalle et al. 2018), we tried to mask nearby stars and to correct galaxy magnitudes. However, the strong contamination affected more than half of the galaxy light contributions and made it difficult to obtain accurate magnitude estimates. Thus, the results were in general not reliable, and we decided not to correct in the present study for stellar contamination. In addition, the cases with a high number of nearby stars, especially those for small objects, were not considered in this work. In contrast, the cases with little contamination were included in the analysis without any correction, resulting in brighter magnitudes. Following Baravalle et al. (2018), we obtained the photometric and structural parameters of these galaxies, including the $R_{1/2}$, C, ellipticity, and the spheroid Sérsic index (n, Sersic 1968).

Appendix A includes useful information that characterizes the VVV tiles of the Galactic disc. For all the tiles, the median interstellar extinctions using the values close to the extended sources, extragalactic sources and galaxies are $A_{Ks} = 1.423$, 0.656, and 0.710 mag, respectively. In general, the extended objects are distributed across the tiles, and the extragalactic sources and galaxies were found mainly in the regions with lower interstellar extinctions. We also used the stellar density defined as the logarithm of the number of stars with $K_s < 15$ mag deg^{-2}, using the PSF photometry of Alonso-García et al. (2018).

Fig. 2 shows the distribution of median A_{Ks} interstellar extinctions defined by extended sources in the upper panels, and displays the stellar densities in the bottom panels. The distributions are presented in the left-hand panels, and the number of detected galaxies per tile as a function of these median A_{Ks} interstellar extinctions and stellar densities is shown in the right-hand panels. At lower interstellar extinctions ($A_{Ks} < 1$ mag), the highest number of detected galaxies is 157, while for $1 \leq A_{Ks} \leq 3$ mag, the number drops from 68 to 1. The median stellar density in the VVV disc, given by log (N_*/deg^2), is 5.066 ± 0.167, which is higher than the peak of the distribution of about 4.5 reported by Schröder et al. (2019a) in the ZoA sample. These results show severe contamination in our studied regions. As expected, as shown in the right-hand panels, the highest number of galaxy detections were obtained in the outermost parts of the disc and the lowest values were found in regions with high interstellar extinction and stellar contamination. No extragalactic candidates were detected in the d100, d108, or d110 tiles. After the visual inspections, all the extragalactic sources in the d065, d069, d070, d071, d072, d073, d099, d100, d101, d102, d108, d109, d110, d112, and d114 tiles were classified as false detections. These regions have lower Galactic latitudes and mainly higher interstellar extinctions, with star crowding being extreme with median A_{K_s} values from 3 up to 6.19 mag and logarithmic stellar densities from 5.055 up to 5.384.

[2]http://horus.roe.ac.uk/vsa

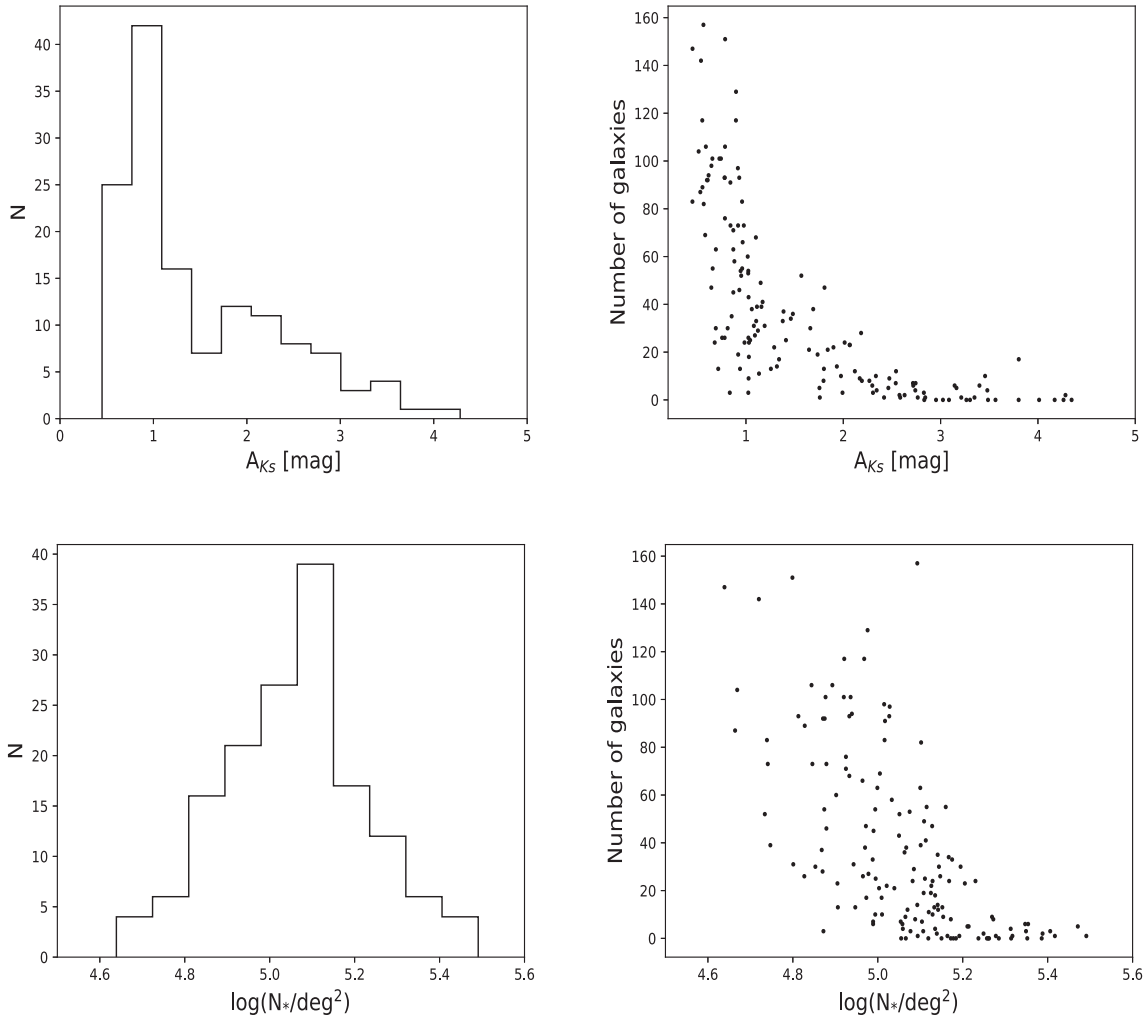

Figure 2. VVV tiles in the Galactic disc showing the distributions of the median A_{Ks} interstellar extinction obtained for all the extended objects detected in the tiles (upper panels) and the stellar density estimates (bottom panels). Left-hand panels display the distributions, and the right-hand panels show the number of galaxy detections for each tile as a function of the extended median A_{Ks} and the stellar density.

On the other hand, more than 150 galaxies were found in the d022 and d122 tiles, with lower interstellar extinctions of 0.56 and 0.79 mag and logarithmic stellar densities of 5.093 and 4.799, respectively.

We also have repeated objects, mostly found in the overlapping tile boundaries due to the observing procedure and tile construction. Within the angular separations of 0.75 arcsec, 122 duplicated galaxies were found. Fig. 3 shows the differences in the coordinates and K_s magnitudes for these duplicated sources. The median differences after 1σ clipping are ΔRA cos(Dec.) $= (-0.062 \pm 0.060)$ arcsec, ΔDec. $= (0.009 \pm 0.066)$ arcsec, and $\Delta K_s = (0.009 \pm 0.102)$ mag. These values might be considered the uncertainty estimates for the astrometry and photometry.

2.1.3 Photometric results

The different NIR photometric systems in general did not match exactly, as was expected, given that the observations were carried out at different sites with different telescopes, IR cameras, detectors, and filters. We used the photometric transformations detailed in Soto et al. (2013) to translate our magnitudes to the 2MASS photometric system. The transformations were obtained on a tile by tile basis, and these were based on the selection of stars with a good photometry. Briefly, the procedure can be summarized as follows: First, the K_s VVV photometry was used to clean the CASU catalogue of non-stellar sources by selecting stars in a specific intensity range, weighted by second moments. Subsequently, stars in relative isolation were selected by using a radius of 2 arcsec to remove multiple sources in close proximity. This VVV catalogue was then cross-referenced with 2MASS sources, with the signal-to-noise ratio greater than 7, and the result was then matched with the VVV catalogue with a small radius of 0.1 arcsec in the J and H passbands. The resulting clean VVV–2MASS catalogue was then used to derive the photometric transformations using a linear fit with an iterative clipping algorithm and adaptive bins. The VVV aperture and total magnitudes of the detected galaxies in the Galactic disc were transformed to the 2MASS photometric system using Soto et al. (2013).

For the detected galaxies, Fig. 4 shows the K_s° magnitudes and the half-light radius as a function of the A_{Ks} interstellar extinctions and stellar densities. The estimated stellar density was defined here as the number of stars with K_s° <15 mag in an area of ∼43 arcmin^2 around each galaxy scaled to an area of 1 deg^2. The median value is $\log(N_*/\mathrm{deg}^2) = 4.933 \pm 0.154$, which as expected was significantly larger than the values reported in surveys based on the 2MASS data

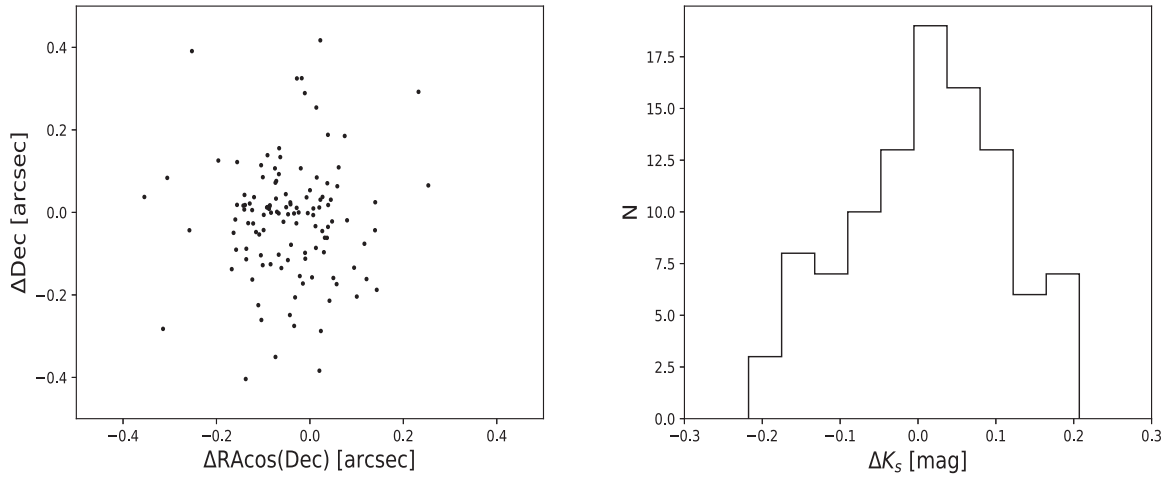

Figure 3. Astrometric and magnitude differences for duplicate galaxies. Left-hand panel shows differences in the coordinates and right-hand panel displays the distribution of the K_s differences.

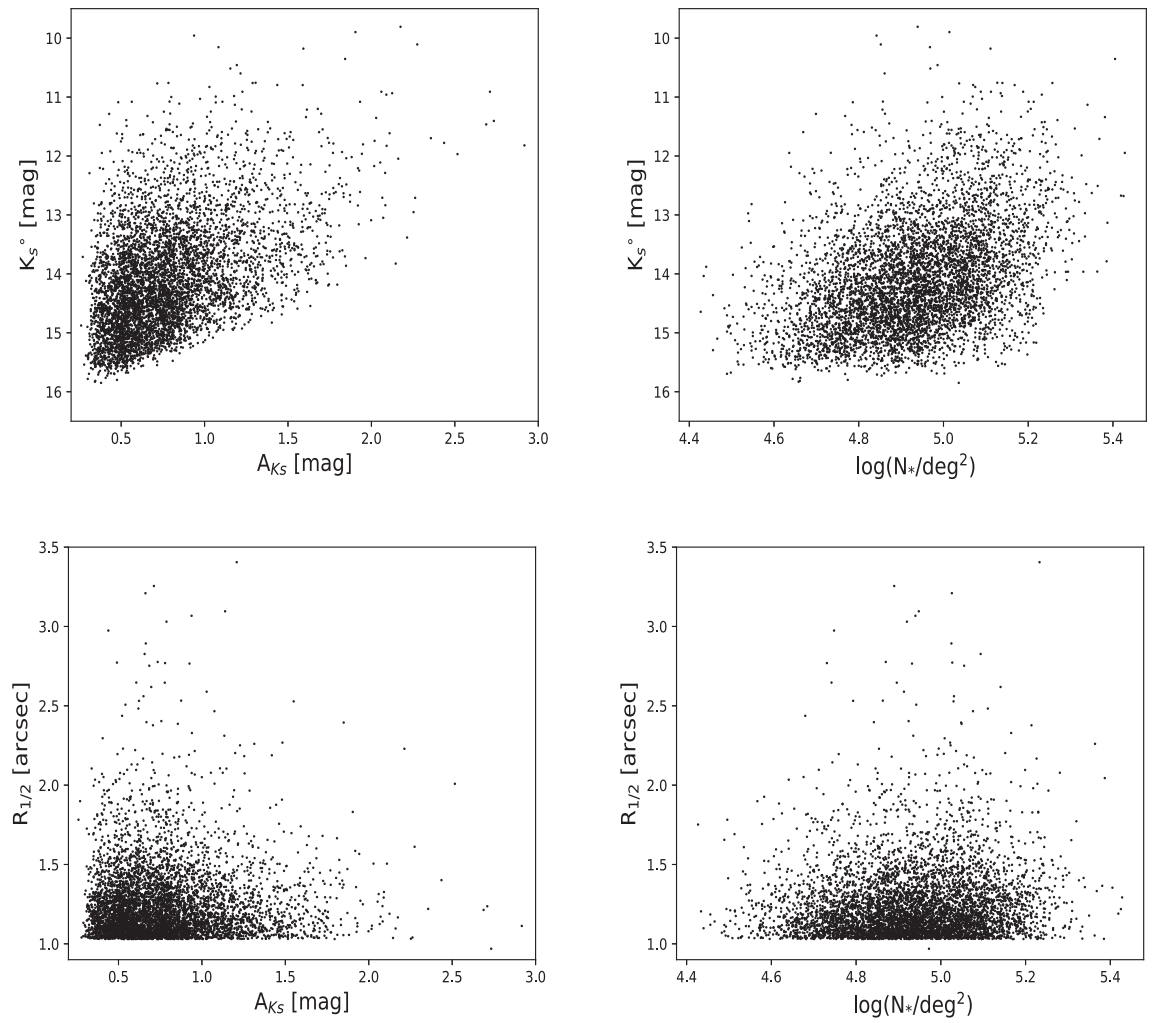

Figure 4. Upper panels show the extinction-corrected K_s° magnitudes as a function of their A_{Ks} interstellar extinctions (left) and stellar density (right). Bottom panels show the size $R_{1/2}$ as a function of these parameters.

Table 1. Median J, H, and K_s magnitude differences.

Literature	ΔJ (mag)	ΔH (mag)	ΔK_s (mag)
2MASS PSC	-0.20 ± 0.52 (18)	-0.19 ± 0.14 (15)	-0.09 ± 0.11 (14)
K_{20} (2MASX)	2.13 ± 0.64 (4)	1.44 ± 0.64 (16)	1.46 ± 0.47 (17)
MAG_AUTO (Schröder et al. 2007)	1.24 ± 0.18 (5)	–	1.01 ± 0.24 (8)
K_{20} (Said et al. 2016)	1.82 ± 0.40 (15)	1.53 ± 0.31 (13)	1.62 ± 0.60 (21)

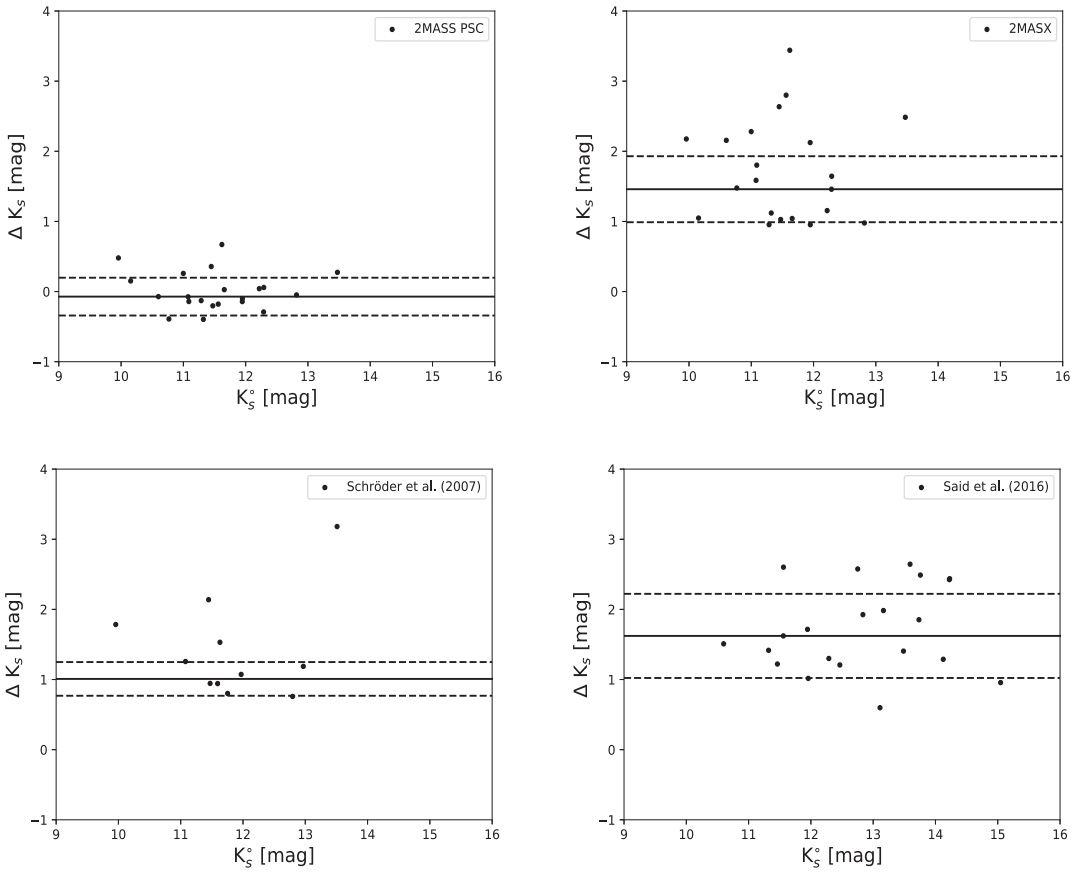

Figure 5. Magnitude comparisons in the K_s passband for galaxies in common for our magnitudes and 2MASS (PSC), 2MASX (K_{20}) (Schröder et al. 2007, MAG_AUTO and Said et al. 2016, K_{20}). Solid lines represent the median differences quoted in Table 1, and dashed lines show the 1σ dispersion.

that cover higher Galactic latitudes. It is clear that we reached K_s° magnitudes of about 15.5 mag in regions with lower interstellar extinctions and stellar densities. In all, 96 per cent of the detections had an $R_{1/2}$ value of about 1.18 arcsec for A_{Ks} interstellar extinctions smaller than 1.5 mag, which then reached median values of 1.22 arcsec. We saw a tendency for brighter galaxies to be observed in regions which displayed higher stellar densities, while at the same time, the size of the detected galaxies did not reveal a clear correlation. In Baravalle et al. (2018), we analysed the completeness of the K_s photometry for the two studied tiles: d010 and d115. At $K_s^\circ = 15.5$ mag, we attained a completeness of 80 and 95 per cent (see their fig. 3) for these tiles, respectively. Comparing the extinctions, the d115 tile had the lowest A_{Ks} values. A conservative completeness of 80 per cent might be estimated at these faint magnitude levels. These results show that both interstellar extinction and stellar density are the main limitations and critical concerns for the detection of galaxies at these low Galactic latitudes.

2.2 Comparison with NIR surveys

Over the VVV disc region, 185 extended sources from the 2MASX were recovered and visually checked. These comprise 21 galaxies and 164 Galactic objects that are: bright single and double stars or stellar associations and gas and dust regions. In Appendix B, we describe these 2MASX sources by dividing them into these categories. We found that about 16 per cent of the Galactic objects have no previous description in the literature. Our galaxies were cross-matched with the 21 galaxies detected by 2MASX using angular separations of about 2 arcsec. Some examples of the common galaxies between the two surveys are shown in Fig. 1. The median astrometric differences after 1σ clipping between the positions of the VVV galaxies and 2MASX are very small: ΔRA cos(Dec.) = (0.087 ± 0.333) arcsec and ΔDec. = (0.036 ± 0.372) arcsec. The galaxies with higher differences are those with a strong contamination by nearby stars.

In this VVV region, there are 22 galaxies reported from Schröder et al. (2007), 41 from Williams et al. (2014), 46 from Said et al.

Table 2. The VVV NIRGC.

ID	RA (J2000)	Dec. (J2000)	l (deg)	b (deg)	A_{Ks} (mag)	J° (mag)	H° (mag)	K_s° (mag)	$J^{\circ}_{2''}$ (mag)	$H^{\circ}_{2''}$ (mag)	$K_s{}^{\circ}_{2''}$ (mag)	$R_{1/2}$ (arcsec)	C	ϵ	n	*WISE* flag
VVV-J113548.43−635434.3	11:35:48.43	−63:54:34.3	294.7325	−2.2484	0.82	15.11	14.69	14.36	15.89	15.42	15.26	1.18	2.64	0.31	1.19	0
VVV-J113550.51−634933.7	11:35:50.51	−63:49:33.7	294.7119	−2.1673	0.91	15.28	14.42	13.90	16.47	15.51	15.10	1.46	2.81	0.57	2.48	0
VVV-J113550.71−635444.0	11:35:50.71	−63:54:44.0	294.7371	−2.2497	0.82	16.68	16.08	15.29	16.95	16.45	16.17	1.12	2.12	0.46	3.50	0
VVV-J113636.55−635556.4	11:36:36.55	−63:55:56.4	294.8234	−2.2449	0.88	16.19	15.43	14.98	16.63	16.02	15.83	1.12	2.36	0.47	2.28	0
VVV-J113722.99−635650.0	11:37:22.99	−63:56:50.0	294.9092	−2.2350	0.90	15.59	15.20	15.10	16.52	16.08	15.93	1.14	3.15	0.60	7.62	0
VVV-J113851.89−635321.8	11:38:51.89	−63:53:21.8	295.0494	−2.1339	1.47	14.69	14.03	13.86	15.76	15.18	14.94	1.25	2.14	0.20	0.42	0
VVV-J113905.29−635803.6	11:39:05.29	−63:58:03.6	295.0947	−2.2023	0.82	15.77	15.00	14.71	16.22	15.70	15.56	1.12	2.55	0.38	1.64	0
VVV-J113926.76−635711.6	11:39:26.76	−63:57:11.6	295.1285	−2.1776	0.82	15.43	14.90	14.59	16.07	15.58	15.36	1.05	2.32	0.35	1.52	0
VVV-J113946.21−640120.3	11:39:46.21	−64:01:20.3	295.1817	−2.2342	0.59	16.38	15.78	15.33	16.78	16.29	16.14	1.11	2.10	0.10	3.82	0
VVV-J114000.97−625333.3	11:40:00.97	−62:53:33.3	294.8991	−1.1400	0.91	14.65	14.10	14.08	15.53	14.85	14.85	1.04	2.30	0.41	3.03	0

(2016), and 19 from Schröder et al. (2019a). Of these galaxies, we have 12 galaxies in common with Schröder et al. (2007), 20 with Williams et al. (2014), 22 with Said et al. (2016), and 19 with Schröder et al. (2019a). In total, after the cross-match, we have 45 galaxies in common with other authors (11 with only one, 25 with two, 5 with three, and 4 with four authors). We visually checked all the objects, including those that were not detected with our procedure (which are diffuse objects, faint galaxies, objects with strong contamination by bright stars or not included in our colour criteria).

Our magnitudes were only transformed to the 2MASS photometric system (Soto et al. 2013) and compared with 2MASS and 2MASX (Schröder et al. 2007; Said et al. 2016). The galaxies reported by Schröder et al. (2019a) have 2MASX photometry, and those of Williams et al. (2014) are included in Said et al. (2016). From these, we used 2MASS aperture magnitudes at a fixed radius aperture of 4 arcsec (2MASS PSC), the isophotal magnitudes within the $K_s = 20$ mag arcsec^{-2} (K_{20}) fiducial elliptical aperture from 2MASX and Said et al. (2016), and MAG_AUTO magnitudes from Schröder et al. (2007).

The magnitude differences were calculated from our total and literature magnitudes ($\Delta m = m$(VVV) $- m$(literature)) for the J, H, and K_s passbands, and the statistical differences are the result of 2σ clipping. Table 1 shows the median magnitude differences in the J, H, and K_s passbands, and includes the final number of objects considered after the σ clipping in parenthesis. The number of compared galaxies for K_s is higher than those for J and H. In some cases, the authors did not present estimates for the magnitudes in these passbands or the differences are higher than the 2σ clipping. Fig. 5 shows only the comparisons for the K_s° magnitudes, as it is the most reliable passband. In general, the uncertainties are important and might be a result of stellar contamination. The best comparisons are with 2MASS magnitudes, and we conclude that our total magnitude estimates are comparable with those that are aperture magnitudes within a fixed aperture of 4 arcsec radius. The comparison with the isophotal K_s magnitudes yielded offsets higher than one magnitude in all cases. We attribute these observed offsets to the different photometric methods, the different procedures used to define the centre positions and magnitudes, and the stellar contamination in these dense regions with high interstellar extinctions.

2.3 Correlation with MIR data

The *Wide-field Infrared Survey Explorer* mission (*WISE*, Wright et al. 2010) mapped the whole sky in the MIR (3.4, 4.6, 12, and 22 μm) passbands. For red sources such as galaxies with older stellar populations, *WISE* goes 1 mag deeper than the 2MASS K_s magnitude for the 3.4 μm passband (Wright et al. 2010). *WISE* also detects the most luminous galaxies in the Universe, such as the ultraluminous IR galaxies which might be related to mergers that lead to dust-enshrouded star formation (Su et al. 2013). In addition, they might be related to active galactic nuclei (AGNs) activity, such as gas disturbed from stable circular orbits and falling into the central supermassive black hole in merging galaxies (Massaro et al. 2012).

In the regions of the VVV disc, we have found 509 galaxies in common with the WISE survey using a cross-match with angular separations of 2 arcsec, implying that 10 per cent of our galaxies have also been seen in the MIR regime by *WISE*.

3 THE VVV NIR GALAXY CATALOGUE

We created the VVV NIRGC, which contains 5563 galaxies across an area of 220 deg^2 within $295^{\circ} < l < 350^{\circ}$ and $-2.25^{\circ} < b <$

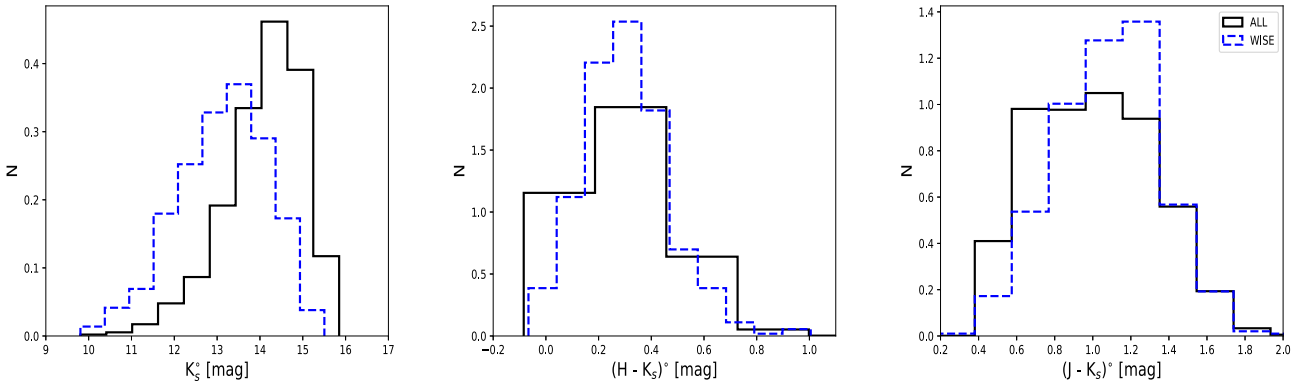

Figure 6. Normalized distributions of the photometric parameters of the galaxies in the VVV NIRGC. The panels show, from left to right, the histograms for K_s° magnitudes and the $(H - K_s)^\circ$ and $(J - K_s)^\circ$ NIR colours. All the galaxies in the catalogue and those also with *WISE* data are shown in solid and dashed histograms, respectively.

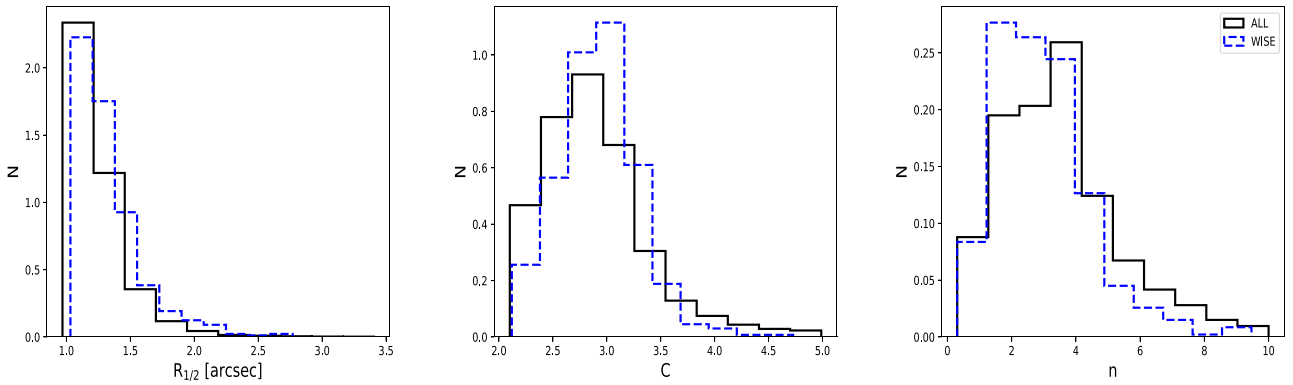

Figure 7. Normalized distributions of morphological parameters of the galaxies in the VVV NIRGC. The panels show, from left to right, the histograms of half-light radius $R_{1/2}$, the concentration index C, and the Sérsic index n. All the galaxies in the catalogue and those also with *WISE* data are shown in solid and dashed histograms, respectively.

Table 3. Median photometric and structural parameters of the galaxies in the VVV NIRGC.

Parameter	All galaxies	Galaxies with *WISE* data
K_s° (mag)	14.24 ± 0.92	13.22 ± 1.06
$(J - K_s)^\circ$ (mag)	0.99 ± 0.31	1.09 ± 0.28
$(H - K_s)^\circ$ (mag)	0.28 ± 0.19	0.30 ± 0.16
$R_{1/2}$ (arcsec)	1.18 ± 0.23	1.27 ± 0.27
C	2.83 ± 0.49	2.92 ± 0.36
n	3.34 ± 1.81	2.79 ± 1.47

+2.25°, using the procedure detailed in the previous section. In this region, we have only a total of 45 galaxies in common with other NIR surveys, such as the 2MASX (Schröder et al. 2007; Williams et al. 2014; Said et al. 2016) catalogues. Consequently, in VVV NIRGC, about 99 per cent of the galaxies are new discoveries.

Table 2 shows the first ten galaxies of VVV NIRGC, listing the identification in column (1), the J2000 equatorial coordinates in columns (2) and (3), the Galactic coordinates in columns (4) and (5), the A_{Ks} interstellar extinction in column (6), total extinction-corrected J°, H°, and K_s° magnitudes in columns (7)–(9), the extinction-corrected J°, H°, and K_s° aperture magnitudes within a fixed aperture of 2 arcsec diameter in columns (10)–12), the morphological parameters: $R_{1/2}$, C, ellipticity, and n in columns (13)–(16), and the *WISE* flag in column (17). If the galaxy has a *WISE* counterpart, this flag is set to 1, otherwise it is set to 0. All magnitudes were extinction-corrected and transformed to the 2MASS photometric system. This table is available in its entirety in a machine-readable form.[3]

Fig. 6 shows the normalized distributions of the reddening corrected K_s° magnitudes and the $(H - K_s)^\circ$ and $(J - K_s)^\circ$ colours of the galaxies in the VVV NIRGC. Fig. 7 also shows the normalized distributions of some of the structural properties for the galaxies, such as $R_{1/2}$, C, and Sérsic index. We made a distinction between galaxies from the VVV NIRGC (represented with solid lines) and those that also have *WISE* data (represented with dashed lines) see Section 2.3. Table 3 summarizes the median values of the photometric and structural parameters for the two normalized distributions. For the galaxies in VVV NIRGC, the limiting K_s° magnitude reaches about 16 mag and the distribution of $(J - K_s)^\circ$ is nearly constant between 0.5 and 1.2 mag. These are small objects with distributions that have peaks with $R_{1/2} \sim 1.3$ arcsec, C with a value of approximately 3, and n around 4. These results are similar to those found in the tiles analysed in Baravalle et al. (2018, 2019), which are characteristic of early-type galaxies. The galaxies with *WISE* data are brighter and with slightly larger sizes with a smaller Sérsic index than the

[3] https://catalogs.oac.uncor.edu/vvv_nirgc/

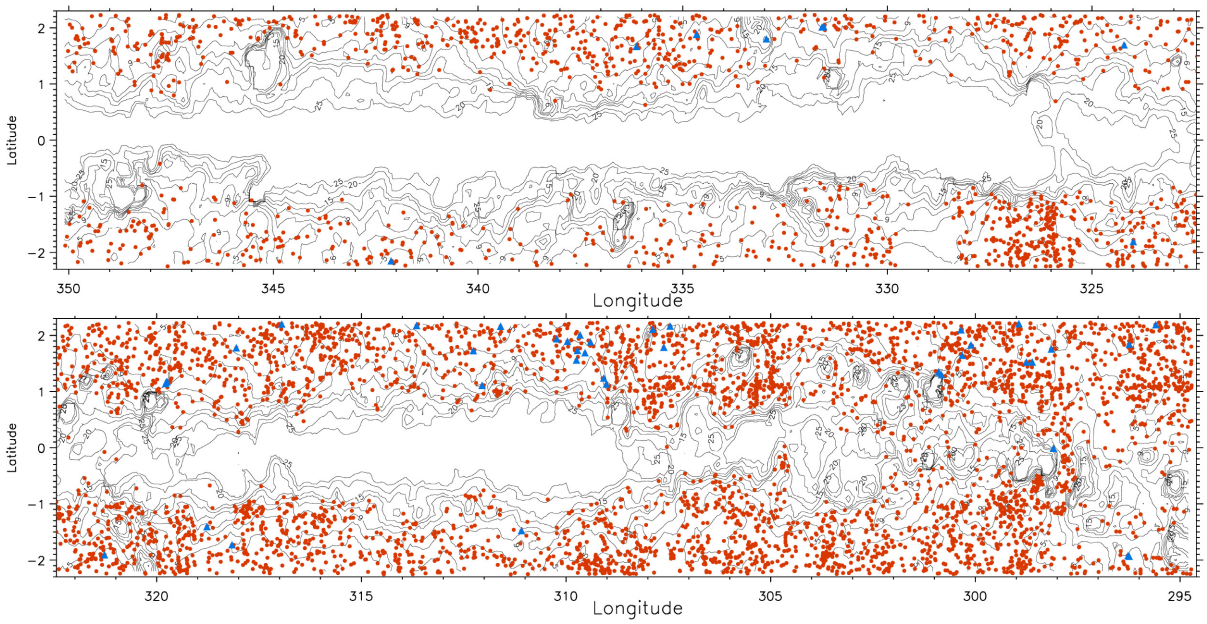

Figure 8. Distribution of galaxies in the VVV disc region superimposed with the A_V contours (1, 3, 5, 7, 9, 11, 13, 15, 20, and 25 mag) derived from the extinction map by Schlafly & Finkbeiner (2011). The galaxies from the VVV NIRGC catalogue are represented with red circles, and those in common with other surveys, such as 2MASX (Schröder et al. 2007; Williams et al. 2014; Said et al. 2016; Schröder et al. 2019a), are shown with blue triangles. For a better visualization, the stellar density grey-scale map was constructed by including all VVV stellar detections.

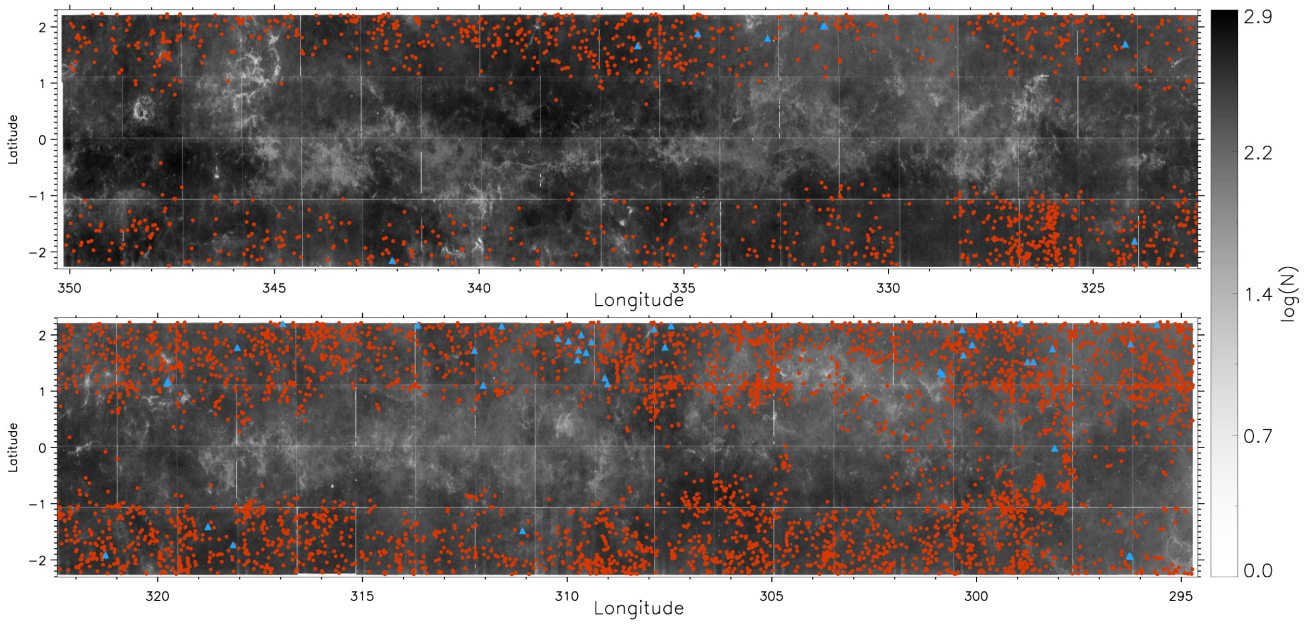

Figure 9. Distribution of galaxies in the VVV disc region superimposed with the stellar density grey-scale map from the catalogues by Alonso-García et al. (2018). As in previous figure, the galaxies from the VVV NIRGC catalogue are represented with red circles and those from other surveys with blue triangles.

galaxies, in general, in the VVV NIRGC. These results might be a consequence of the predominance of late-type galaxies.

3.1 The galaxy distribution map

Figs 8 and 9 show the distribution of the 5563 galaxies in the VVV NIRGC catalogue with the superposition of the A_V contours (1, 3, 5, 7, 9, 11, 13, 15, 20, and 25 mag) derived from the extinction map by Schlafly & Finkbeiner (2011) and the stellar density grey-scale map from the VVV catalogues by Alonso-García et al. (2018), respectively. The star count map has a pixel scale of 0.9 arcmin^2 and includes all stellar detections, regardless of their magnitudes, for a better visualization. The galaxies in the VVV region across the Southern Galactic plane are represented by red circles. We have also included the galaxies in common with previous works: 2MASX (Schröder et al. 2007; Williams et al. 2014; Said et al. 2016) with blue triangles. In general, the regions with strong interstellar extinction or a higher stellar density have no galaxy detections.

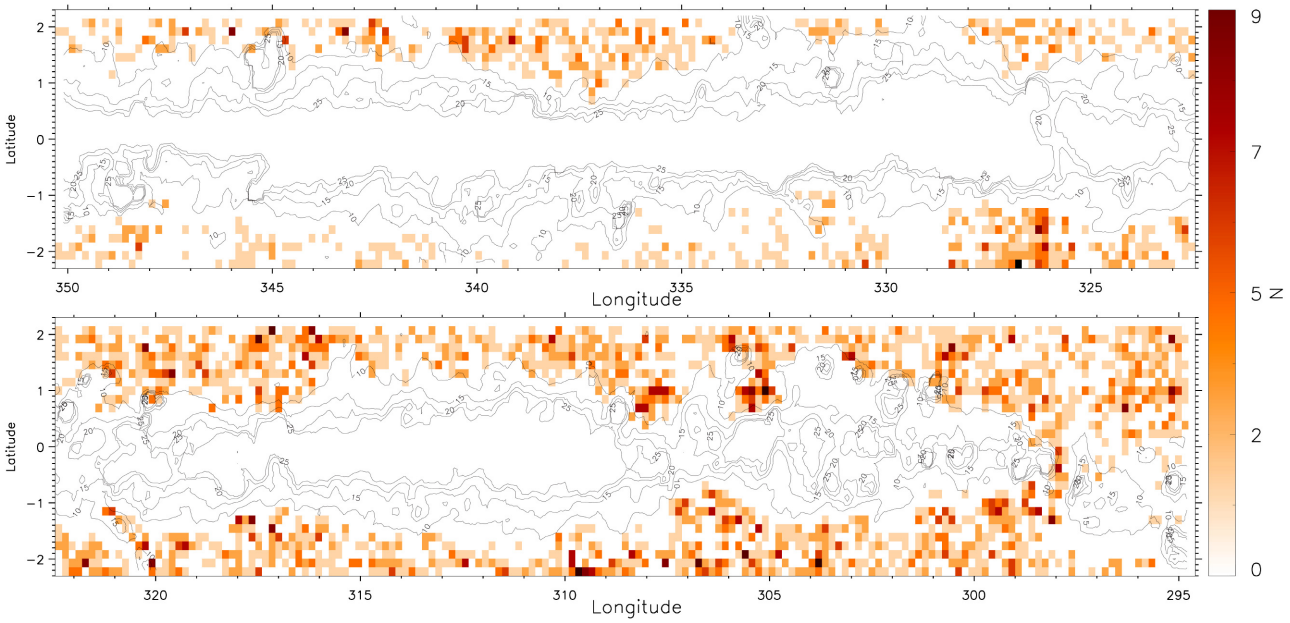

Figure 10. Distribution of the brightest galaxies ($K_s^\circ < 15$ mag) in the VVV disc region. The density plot has been calculated at a resolution of 90 arcmin^2 pixel^{-1} and shows the superposition of A_V contours (10, 15, 20, and 25 mag) from Schlafly & Finkbeiner (2011).

There are 3584 galaxies brighter than $K_s^\circ = 15$ mag in regions of low interstellar extinction, $A_{Ks} < 1$ mag. This number represents about 64 per cent of the galaxies in the VVV NIRGC catalogue. Fig. 10 shows the distribution of these brightest galaxies as a density plot with a resolution of 90 arcmin^2 pixel^{-1}, together with the superposition of some A_V contours (10, 15, 20, and 25 mag) from Schlafly & Finkbeiner (2011). In Figs 8–10, possible clustering can be appreciated at different areas of the map. These regions in Galactic coordinates, in order of density, are the following: (326.0°, −1.4°), (326.7°, −2.1°), (299.2°, −1.0°), (305.0°, 1.0°), (308.0°, 1.2°), (309.3°, −2.0°), (317.0°, 2.0°), and (300.8°, 1.8°). The galaxy cluster VVV-J144321−611754, identified in Baravalle et al. (2019), is located in a less dense region (the d015 tile, $l = 315.8°$ and $b = -1.6°$). As it is very important to know which of these observed overdensities of galaxies are real structures, additional observations, that is, NIR spectroscopy, are needed in order to select and confirm the galaxy cluster candidates.

The VVV NIRGC is the largest collection available to date of galaxies in the Galactic plane within $295° < l < 350°$ and $-2.25° < b < +2.25°$. In general, dense regions of galaxies are related to lower interstellar extinctions and stellar densities in the Galactic plane. Thus, Figs 8–10 show that the galaxy distribution closely resembles the distribution of low extinction in the NIR interstellar extinction maps made by the VVV survey (Minniti et al. 2018; Soto et al. 2019).

Indeed, the main factors driving galaxy detection in the VVV images are the real distribution of galaxies and the total interstellar extinction and stellar density throughout the MW plane. The windows of low extinction, in particular, contain a higher number of galaxies per unit area. In fact, this is a useful method for identifying low extinction windows across the MW disc. Some other secondary factors that favour the detection (or non-detection) of galaxies in the VVV survey are the seeing and the sky brightness variations in the NIR, as discussed earlier. For instance, it is more difficult to detect faint galaxies in the crowded regions near the Galactic bulge or along the MW spiral arm tangents.

4 MAIN CONCLUSIONS AND FUTURE WORK

In this work, we have analysed the VVV NIR images across the Southern Galactic plane in order to search for galaxies using SExtractor+PSFEx, as described in Baravalle et al. (2018). We found that the main limitations for galaxy detections are both the high interstellar extinction and the strong star crowding, which are extremely severe in some cases.

The VVV NIRGC comprises the photometric and morphological properties of 5563 visually confirmed galaxies, with 99 per cent of these having no previous identification. This work compiles the largest collection to date of galaxies in the Galactic disc (within $295° < l < 350°$ and $-2.25° < b < +2.25°$).

We have compared galaxy magnitudes with other NIR surveys in the ZoA, namely 2MASS and 2MASX (Schröder et al. 2007; Said et al. 2016), and our total magnitude estimates are comparable with the 2MASS magnitudes. The comparison with other isophotal K_s magnitudes have offsets higher than 1mag in all cases (Table 1). These differences might be due to the different photometric methods and procedures used to define the magnitudes in these dense regions with high interstellar extinctions. The total number of 185 2MASX extended objects were visually inspected. The 21 galaxies in common were used for the comparisons, and the remaining 164 extended objects were re-classified as detailed in Appendix B.

The confirmed galaxies in the VVV NIRGC have colours and morphological parameters that are consistent with early-type galaxies (Table 3). The galaxies with MIR data from *WISE* are about 10 per cent of the sample and showing some differences with the total distributions. These are, in general, brighter and larger objects with a smaller Sérsic index than the galaxies in the VVV NIRGC. Thus, they might be late-type galaxies.

We have also presented the galaxy distribution map across the Southern Galactic plane using the VVV NIRGC. In general, the dense regions of galaxies are related to lower interstellar extinctions in the Galactic plane. These results confirm that both the interstellar extinction and stellar density are the main limitations for these

studies at lower Galactic latitudes. This work represents the first step in exploring the distribution of galaxies in the ZoA using the VVV survey. The VVV NIRGC may also be used to identify candidate compact groups and clusters of galaxies, which require later spectroscopic confirmation.

In the future, our procedure might be improved by using co-added images to reach fainter objects and, most importantly, be extended to the VVVX area. It is very important to cross-correlate with surveys using other frequencies, such as the Galactic Legacy Infrared Mid-Plane Survey Extraordinaire (Benjamin et al. 2005) and *WISE* MIR data, the Widefield Australian Square Kilometer Array Pathfinder L-band legacy all-sky blind survey (Koribalski et al. 2020) of neutral hydrogen, and X-ray and radio source catalogues.

ACKNOWLEDGEMENTS

We would like to thank the anonymous referee for the useful comments and suggestions which has helped to improve this paper. This work was partially supported by Consejo de Investigaciones Científicas y Técnicas (CONICET) and Secretaría de Ciencia y Técnica de la Universidad Nacional de Córdoba (SECyT). We gratefully acknowledge data from the ESO Public Survey program ID 179.B-2002 taken with the VISTA telescope, and products from the CASU. DM is supported by the BASAL Center for Astrophysics and Associated Technologies (CATA) through grant AFB 170002 and by Proyecto FONDECYT no. 1170121. This research has made use of the NASA/IPAC Infrared Science Archive, which is funded by the National Aeronautics and Space Administration and operated by the California Institute of Technology. This publication makes use of data products from the 2MASS, which is a joint project of the University of Massachusetts and the Infrared Processing and Analysis Center California Institute of Technology, funded by the National Aeronautics and Space Administration and the National Science Foundation. This research has made use of the VizieR catalogue access tool, CDS, Strasbourg, France (doi:10.26093/cds/vizier). The original description of the VizieR service was published in 2000, A&AS 143, 23.

DATA AVAILABILITY

The data underlying this article are available in the IATE home page at https://catalogs.oac.uncor.edu/vvv_nirgc/.

REFERENCES

Alonso-García J. et al., 2018, A&A, 619, A4
Amôres E. B. et al., 2012, AJ, 144, 127
Amôres E. B., Lépine J. R. D., 2005, AJ, 130, 659
Amôres E. B., Lépine J. R. D., 2007, AJ, 133, 1519
Araya E., Hofner P., Kurtz S., Bronfman L., DeDeo S., 2005, ApJS, 157, 279
Arce H. G., Goodman A. A., 1999, ApJ, 512, L135
Baravalle L. D. et al., 2019, ApJ, 874, 46
Baravalle L. D., Alonso M. V., Nilo Castellón J. L., Beamín J. C., Minniti D., 2018, AJ 155, 46
Barbá R. H. et al., 2015, A&A, 581, A120
Beamín J. C. et al., 2013, A&A, 557, L8
Beltrán M. T., Brand J., Cesaroni R., Fontani F., Pezzuto S., Testi L., Molinari S., 2006, A&A, 447, 221
Benjamin R. A. et al., 2005, ApJ, 630, L149
Bertin E., 2011, in Evans I. N., Accomazzi A., Mink D. J., Rots A. H., eds, ASP Conf. Ser. Vol. 442, Astronomical Data Analysis Software and Systems XX. Astronomical Society of the Pacific, San Francisco, p. 435
Bertin E., Arnouts S., 1996, A&AS (Journal), 117, 393
Borissova J. et al., 2011, A&A, 532, A131
Borissova J. et al., 2014, A&A, 569, A24
Bronfman L., Nyman L. A., May J., 1996, A&AS, 115, 81
Caratti o Garatti A., Stecklum B., Linz H., Garcia Lopez R., Sanna A., 2015, A&A, 573, A82
Caswell J. L. et al., 2010, MNRAS, 404, 1029
Caswell J. L., Haynes R. F., Goss W. M., 1977, MNRAS, 181, 427
Catelan M. et al., 2011, in McWilliam A., ed., RR Lyrae Stars, Metal-Poor Stars, and the Galaxy, Vol. 5, The Observatories of the Carnegie Institution of Washington, Pasadena, CA, p. 145
Churchwell E. et al., 2006, ApJ, 649, 759
Coldwell G., Alonso S., Duplancic F., Hempel M., Ivanov V. D., Minniti D., 2014, A&A, 569, A49
Conselice C. J., Bershady M. A., Jangren A., 2000, ApJ, 529, 886
Contreras Y. et al., 2013, A&A, 549, A45
Courtois H. M., Tully R. B., 2015, MNRAS, 447, 1531
Courtois H. M., Tully R. B., Fisher J. R., Bonhomme N., Zavodny M., Barnes A., 2009, AJ, 138, 1938
Culverhouse T. et al., 2011, ApJS, 195, 8
Cutri R. M. et al., 2003, VizieR On-line Data Catalog: II/328. Originally published in: IPAC/Caltech (2013)
Cyganowski C. J. et al., 2008, AJ, 136, 2391
Dalton G. B. et al., 2006, in McLean I. S., Iye M., eds, Proceedings of the SPIE, Volume 6269. p. 62690X
Dutra C. M., Bica E., Soares J., Barbuy B., 2003, A&A, 400, 533
Egan M. P. et al., 2001, CDS/ADC Collection of Electronic Catalogues, 5107, 0
Egan M. P. et al., 2003, VizieR Online Data Catalog, p. V/114
Emerson J., McPherson A., Sutherland W., 2006, The Messenger, 126, 41
Epchtein N. et al., 1997, The Messenger, 87, 27
Frew D. J., Bojičić I. S., Parker Q. A., 2013, MNRAS, 431, 2
Garay G., Brooks K. J., Mardones D., Norris R. P., 2006, ApJ, 651, 914
Garay G., Mardones D., Brooks K. J., Videla L., Contreras Y., 2007, ApJ, 666, 309
Giveon U., Sternberg A., Lutz D., Feuchtgruber H., Pauldrach A. W. A., 2002, ApJ, 566, 880
Gladders M. D., Yee H. K. C., 2000, AJ, 120, 2148
Gonzalez O. A., Rejkuba M., Zoccali M., Valenti E., Minniti D., Schultheis M., Tobar R., Chen B., 2012, A&A, 543, A13
Goss W. M., Shaver P. A., 1970, Aust. J. Phys. Astrophys. Suppl., 14, 1
Gum C. S., 1955, MmRAS, 67, 155
Guzmán A. E. et al., 2014, ApJ, 796, 117
Guzmán A. E., Garay G., Brooks K. J., Voronkov M. A., 2012, ApJ, 753, 51
Harju J., Lehtinen K., Booth R. S., Zinchenko I., 1998, A&AS, 132, 211
Helou G., Walker D. W., 1988, Infrared Astronomical Satellite (IRAS) Catalogs and Atlases, 7, 1
Hindson L., Thompson M. A., Urquhart J. S., Faimali A., Johnston-Hollitt M., Clark J. S., Davies B., 2013, MNRAS, 435, 2003
Howlett C. et al., 2017, MNRAS, 471, 3135
Huchra J. et al., 2005, in Fairall A. P., Woudt P. A., eds, ASP Conf. Ser. Vol. 329, Nearby Large-Scale Structures and the Zone of Avoidance. Proceedings of the Conference Held 28 March - 2 April, 2004 in Cape Town, South Africa, p. 135
Huchra J. P. et al., 2012, ApJS, 199, 26
Huchra J. P., Geller M. J., 1982, ApJ, 257, 423
Ishihara D. et al., 2010, A&A, 514, A1
Jarrett T., 2004, PASA, 21, 396
Jarrett T. H., Chester T., Cutri R., Schneider S., 2000a, AJ, 119, 2498
Jarrett T. H., Chester T., Cutri R., Schneider S., 2000b, AJ, 120, 298
Jones C., Dickey J. M., 2012, ApJ, 753, 62
Karachentseva V. E., Mitronova S. N., Melnyk O. V., Karachentsev I. D., 2010, Astrophys. Bull., 65, 1
Kharchenko N. V., Piskunov A. E., Schilbach E., Röser S., Scholz R. D., 2013, A&A, 558, A53
Klypin A., Holtzman J., Primack J., Regos E., 1993, ApJ, 416, 1
Koribalski B. S. et al., 2020, Ap&SS, 365, 118
Kourkchi E., Tully R. B., 2017, ApJ, 843, 16
Kraan-Korteweg R. C., 2000, A&AS (Journal), 141, 123

Kraan-Korteweg R. C., Lahav O., 2000, A&AR, 10, 211
Kraan-Korteweg R. C., Woudt P. A., 1999, PASA, 16, 53
Kraan-Korteweg R. C., Woudt P. A., Cayatte V., Fairall A. P., Balkowski C., Henning P. A., 1996, Nature, 379, 519
Kraan-Korteweg R. C., Cluver M. E., Bilicki M., Jarrett T. H., Colless M., Elagali A., Böhringer H., Chon G., 2017, MNRAS, 466, L29
Kraan-Korteweg R. C., van Driel W., Schröder A. C., Ramatsoku M., Henning P. A., 2018, MNRAS, 481, 1262
Kron R. G., 1980, ApJS, 43, 305
Kuchar T. A., Clark F. O., 1997, ApJ, 488, 224
Kwok S., Volk K., Bidelman W. P., 1997, ApJS, 112, 557
Lambert T. S., Kraan-Korteweg R. C., Jarrett T. H., Macri L. M., 2020, MNRAS, 497, 2954
Macri L. M. et al., 2019, ApJS, 245, 6
Massaro F., D'Abrusco R., Tosti G., Ajello M., Gasparrini D., Grindlay J. E., Smith H. A., 2012, ApJ, 750, 138
Masters K. L., Springob C. M., Huchra J. P., 2008, AJ, 135, 1738
Minniti D. et al., 2010, New A, 15, 433
Minniti D. et al., 2011, A&A, 527, A81
Minniti D. et al., 2017, ApJ, 849, L24
Minniti D. et al., 2018, A&A, 616, A26
Mitronova S. N., Karachentsev I. D., Karachentseva V. E., Jarrett T. H., Kudrya Y. N., 2004, Bull. Spec. Astrophys. Obs., 57, 5
Mookerjea B., Kramer C., Nielbock M., Nyman L. Å., 2004, A&A, 426, 119
Morales E. F. E., Wyrowski F., Schuller F., Menten K. M., 2013, A&A, 560, A76
Mori H., Maeda Y., Furuzawa A., Haba Y., Ueda Y., 2013, PASJ, 65, 102
Mottram J. C., Hoare M. G., Lumsden S. L., Oudmaijer R. D., Urquhart J. S., Sheret T. L., Clarke A. J., Allsopp J., 2007, A&A, 476, 1019
Mutabazi T., Blyth S. L., Woudt P. A., Lucey J. R., Jarrett T. H., Bilicki M., Schröder A. C., Moore S. A. W., 2014, MNRAS, 439, 3666
Nagayama T. et al., 2004, MNRAS, 354, 980
Paturel G., Theureau G., Bottinelli L., Gouguenheim L., Coudreau-Durand N., Hallet N., Petit C., 2003, A&A, 412, 57
Peebles P. J. E., 1980, in James P., Peebles E., eds, The Large-Scale Structure of the Universe, Princeton University Press
Peretto N., Fuller G. A., 2009, A&A, 505, 405
Pichel A. et al., 2020, MNRAS, 491, 3448
Pinheiro M. C., Copetti M. V. F., Oliveira V. A., 2010, A&A, 521, A26
Purcell C. R. et al., 2012, MNRAS, 426, 1972
Robitaille T. P. et al., 2008, AJ, 136, 2413
Robitaille T. P., Cohen M., Whitney B. A., Meade M., Babler B., Indebetouw R., Churchwell E., 2007, AJ, 134, 2099
Roman-Lopes A., Abraham Z., 2006, AJ, 131, 2223
Rousseau J. et al., 2000, A&A, 363, 62
Said K., Kraan-Korteweg R. C., Jarrett T. H., Staveley-Smith L., Williams W. L., 2016, MNRAS, 462, 3386
Saito R. et al., 2010, The Messenger, 141, 24
Saito R. K. et al., 2019, MNRAS, 490, 1171
Saito R. K., Minniti D., Benjamin R. A., Navarro M. G., Alonso-García J., Gonzalez O. A., Kammers R., Surot F., 2020, MNRAS, 494, L32
Schlafly E. F., Finkbeiner D. P., 2011, ApJ, 737, 103
Schlegel D. J., Finkbeiner D. P., Davis M., 1998, ApJ, 500, 525
Schröder A. C., Mamon G. A., Kraan-Korteweg R. C., Woudt P. A., 2007, A&A, 466, 481
Schröder A. C., an Driel W., Kraan-Korteweg R. C., 2019a, MNRAS, 482, 5167
Schröder A. C., Flöer L., Winkel B., Kerp J., 2019b, MNRAS, 489, 2907
Sersic J. L., 1968, Atlas de Galaxias Australes. Observatorio Astronomico, Cordoba, Argentina
Shaver P. A., McGee R. X., Newton L. M., Danks A. C., Pottasch S. R., 1983, MNRAS, 204, 53
Simpson R. J. et al., 2012, MNRAS, 424, 2442
Skrutskie M. F. et al., 2006, AJ, 131, 1163
Sorce J. G., Colless M., Kraan-Korteweg R. C., Gottlöber S., 2017, MNRAS, 471, 3087
Soto M. et al., 2013, A&A, 552, A101
Soto M. et al., 2019, MNRAS, 488, 2650
Staveley-Smith L., Kraan-Korteweg R. C., Schröder A. C., Henning P. A., Koribalski B. S., Stewart I. M., Heald G., 2016, Astron. J., 151, 52
Stephenson C. B., Sanduleak N., 1971, Publ. Warner & Swasey Obs., 1, 1
Su S., Kong X., Li J., Fang G., 2013, ApJ, 778, 10
Suárez O., García-Lario P., Manchado A., Manteiga M., Ulla A., Pottasch S. R., 2006, A&A, 458, 173
Tapia M., Persi P., Roth M., Elia D., Molinari S., Saldaño H. P., Gómez M., 2014, MNRAS, 437, 606
Urquhart J. S. et al., 2014, A&A, 568, A41
Urquhart J. S. et al., 2018, MNRAS, 473, 1059
van Driel W., Schneider S. E., Kraan-Korteweg R. C., Monnier Ragaigne D., 2009, A&A, 505, 29
Vauglin I. et al., 2002, A&A, 387, 1
Vig S., Ghosh S. K., Ojha D. K., Verma R. P., 2007, A&A, 463, 175
Walsh A. J., Bertoldi F., Burton M. G., Nikola T., 2001, MNRAS, 326, 36
West R. M., Tarenghi M., 1989, A&A, 223, 61
Williams W. L., Kraan-Korteweg R. C., Woudt P. A., 2014, MNRAS, 443, 41
Woudt P. A., Kraan-Korteweg R. C., 2001, A&A, 380, 441
Wray J. D., 1966, PhD thesis, Northwestern University
Wright E. L. et al., 2010, AJ, 140, 1868
Yu N., Xu J., 2016, ApJ, 833, 248

APPENDIX A: THE STUDIED VVV TILES IN THE GALACTIC DISC

This is important information for the reader interested in the details of the observed regions. Table A1 shows some characteristics of the studied tiles, with the identification in column (1), the Galactic coordinates and the interstellar extinctions at V passband of the centre in columns (2)–(4), the median K_s interstellar extinctions of the extended objects in column (5), and the number of confirmed galaxies in column (6).

Table A1. VVV tiles in the Galactic disc.

Tile ID	l (deg)	b (deg)	A_V (mag)	A_{K_s} (mag)	Number of galaxies
d001	295.4376	−1.6497	8.703	1.159	39
d002	296.8967	−1.6498	7.858	1.081	31
d003	298.3557	−1.6497	4.725	0.553	89
d004	299.8147	−1.6497	4.988	0.588	106
d005	301.2737	−1.6497	4.226	0.599	92
d006	302.7327	−1.6497	5.747	0.785	106
d007	304.1917	−1.6498	4.745	0.655	101
d008	305.6510	−1.6497	4.261	0.551	117
d009	307.1097	−1.6497	4.298	0.581	69
d010	308.5690	−1.6497	9.103	0.898	129
d011	309.9739	−1.6360	7.218	0.966	66
d012	311.4867	−1.6497	8.587	1.060	38
d013	312.9457	−1.6497	5.891	0.945	54
d014	314.4047	−1.6497	6.705	0.870	63
d015	315.8371	−1.6502	6.113	0.840	91
d016	317.2949	−1.6497	5.116	0.645	98
d017	318.7539	−1.6497	5.909	0.781	93
d018	320.2129	−1.6497	4.319	0.960	83
d019	321.6719	−1.6497	7.393	0.917	97
d020	323.1406	−1.6362	7.693	0.881	58
d021	324.5899	−1.6497	10.229	1.027	43
d022	326.0489	−1.6497	3.653	0.563	157
d023	327.5079	−1.6497	4.355	0.566	82
d024	328.9669	−1.6497	6.620	0.834	3
d025	330.4259	−1.6497	5.124	0.853	35
d026	331.8849	−1.6497	9.314	0.781	26
d027	333.3439	−1.6497	5.381	0.715	13

Table A1 – *continued*

Tile ID	l (deg)	b (deg)	A_V (mag)	A_{K_s} (mag)	Number of galaxies
d028	334.8029	−1.6497	9.009	0.985	24
d029	336.1531	−1.5276	8.087	0.920	19
d030	337.7209	−1.6497	8.056	1.027	9
d031	339.1799	−1.6497	9.367	1.134	11
d032	340.6389	−1.6497	10.498	1.318	14
d033	342.0979	−1.6497	8.322	1.031	24
d034	343.5569	−1.6497	6.974	1.030	18
d035	345.0159	−1.6498	6.417	0.812	30
d036	346.4749	−1.6498	8.109	0.939	13
d037	347.9339	−1.6497	5.365	0.690	30
d038	349.3929	−1.6497	5.398	0.679	24
d039	295.4374	−0.5576	7.001	1.024	3
d040	296.8962	−0.5576	10.775	1.256	13
d041	298.3548	−0.5575	4.748	0.931	93
d042	299.8135	−0.5570	9.725	1.102	68
d043	301.2720	−0.5575	10.005	1.192	31
d044	302.7308	−0.5575	20.385	1.976	10
d045	304.1896	−0.5576	19.626	1.840	21
d046	305.6481	−0.5575	10.511	1.113	39
d047	307.1068	−0.5575	10.236	1.461	34
d048	308.5653	−0.5575	19.512	2.473	9
d049	310.0249	−0.5544	28.317	3.480	4
d050	311.4828	−0.5575	39.246	2.743	7
d051	312.9415	−0.5576	31.868	2.298	6
d052	314.4001	−0.5576	28.625	2.305	3
d053	315.8588	−0.5575	28.934	2.268	8
d054	317.3175	−0.5575	21.962	2.014	24
d055	318.7761	−0.5576	18.618	2.539	7
d056	320.2348	−0.5576	24.226	2.542	12
d057	321.6935	−0.5575	17.682	2.066	23
d058	323.1522	−0.5575	17.893	2.191	8
d059	324.6109	−0.5575	22.517	3.163	5
d060	326.0695	−0.5575	42.993	2.463	5
d061	327.5282	−0.5576	29.493	3.457	10
d062	328.9868	−0.5576	24.148	2.577	2
d063	330.4455	−0.5575	25.052	2.169	9
d064	331.9041	−0.5575	15.324	1.797	8
d065	333.3629	−0.5576	39.527	2.832	0
d066	334.8215	−0.5575	25.793	2.419	1
d067	336.2801	−0.5576	21.919	2.828	3
d068	337.7388	−0.5576	18.504	2.765	1
d069	339.1975	−0.5576	35.709	4.263	0
d070	340.6561	−0.5576	34.913	5.366	0
d071	342.1148	−0.5576	12.754	3.302	0
d072	343.5735	−0.5575	27.715	3.802	0
d073	345.0321	−0.5576	30.089	2.953	0
d074	346.4908	−0.5576	16.443	1.759	1
d075	347.9495	−0.5576	17.169	1.755	5
d076	349.4082	−0.5575	14.235	2.585	1
d077	295.4375	0.5346	7.330	0.781	93
d078	296.8963	0.5346	6.419	0.755	26
d079	298.3552	0.5345	4.322	0.841	73
d080	299.8141	0.5346	11.560	1.386	37
d081	301.2729	0.5346	10.349	1.661	30
d082	302.7318	0.5346	14.507	2.183	28
d083	304.1908	0.5346	17.355	2.067	23
d084	305.6495	0.5346	17.463	1.807	47
d085	307.1084	0.5345	18.849	1.569	52
d086	308.5672	0.5346	33.014	1.691	38
d087	310.0261	0.5346	42.790	3.144	6
d088	311.4849	0.5346	42.121	3.803	17
d089	312.9438	0.5346	26.151	2.716	7
d090	314.4027	0.5346	22.500	2.335	10

Table A1 – *continued*

Tile ID	l (deg)	b (deg)	A_V (mag)	A_{K_s} (mag)	Number of galaxies
d091	315.8616	0.5346	22.336	2.119	12
d092	317.3204	0.5346	13.721	1.482	36
d093	318.7793	0.5346	16.766	1.736	19
d094	320.2382	0.5346	28.764	1.899	22
d095	321.6970	0.5346	12.878	1.934	14
d096	323.1559	0.5346	18.679	2.343	4
d097	324.6148	0.5346	20.111	2.630	2
d098	326.0736	0.5346	25.883	2.842	1
d099	327.5325	0.5346	33.170	4.346	0
d100	328.9913	0.5346	79.078	6.185	0
d101	330.4502	0.5346	47.601	4.172	0
d102	331.9091	0.5346	27.476	3.564	0
d103	333.3679	0.5346	20.665	3.212	1
d104	334.8269	0.5346	16.362	2.740	4
d105	336.2857	0.5346	19.643	2.719	6
d106	337.7445	0.5346	14.083	1.992	3
d107	339.2034	0.5346	24.339	4.283	2
d108	340.6622	0.5346	19.564	3.086	0
d109	342.1212	0.5346	37.578	3.024	0
d110	343.5801	0.5346	28.236	3.265	0
d111	345.0388	0.5346	19.256	3.348	1
d112	346.4977	0.5346	34.060	4.012	0
d113	347.9566	0.5346	22.919	3.399	6
d114	349.4155	0.5346	23.303	3.487	0
d115	295.4380	1.6270	3.520	0.451	147
d116	296.8973	1.6268	4.355	0.531	87
d117	298.3569	1.6268	3.756	0.514	104
d118	299.8156	1.6266	4.546	0.538	142
d119	301.2761	1.6268	3.258	0.450	83
d120	302.7357	1.6268	7.564	0.978	73
d121	304.1952	1.6268	12.774	0.951	52
d122	305.6592	1.6765	41.703	0.786	151
d123	307.1145	1.6268	5.067	0.607	92
d124	308.5740	1.6268	4.553	0.727	101
d125	310.0336	1.6268	7.753	0.919	74
d126	311.4932	1.6268	8.216	0.932	46
d127	312.9528	1.6268	7.704	1.024	54
d128	314.4124	1.6268	7.331	1.018	60
d129	315.8719	1.6268	7.606	0.897	117
d130	317.3316	1.6268	4.509	0.616	94
d131	318.7912	1.6268	6.303	0.784	76
d132	320.2508	1.6268	6.011	0.743	101
d133	321.7104	1.6268	8.537	0.870	71
d134	323.1699	1.6268	6.516	1.025	26
d135	324.6295	1.6268	8.388	1.092	27
d136	326.0891	1.6268	6.649	0.870	45
d137	327.5487	1.6268	11.189	1.378	33
d138	328.3753	1.6268	38.469	1.801	13
d139	330.4679	1.6268	11.014	1.648	21
d140	331.9275	1.6268	9.788	1.411	25
d141	333.3871	1.6268	12.664	1.340	17
d142	334.8467	1.6268	7.171	1.023	53
d143	336.3062	1.6268	5.663	0.691	63
d144	337.7658	1.6268	5.742	0.658	55
d145	339.2255	1.6268	5.136	0.644	47
d146	340.6850	1.6268	11.347	1.171	41
d147	342.1446	1.6268	9.055	1.151	49
d148	343.6042	1.6268	8.695	1.043	25
d149	345.0639	1.6268	47.313	1.290	22
d150	346.5234	1.6268	10.183	1.123	29
d151	347.9830	1.6267	8.418	0.961	55
d152	349.4426	1.6267	9.097	1.105	33

In previous works, Amôres et al. (2012) reported 214 objects in the d003 tile, of which 72 were considered to be possible galaxies. These detections are, in general, in agreement with our observations, with any differences possible arising from the adopted methodology and the removal of objects with strong stellar contamination. Also, Baravalle et al. (2018) reported 530 galaxies in the d010 and d115 tiles. Here, we were more discriminative in the image selection and more exhaustive in the visual inspection.

APPENDIX B: THE 2MASS EXTENDED SOURCES IN THE VVV DISC REGION

In Section 2.2, we reported 185 extended sources from the 2MASX catalogue in the regions of the VVV disc. We visually checked all of these, with this list including 21 galaxies and 164 objects that are mainly stars and stellar associations.

Table B1 shows the 2MASX galaxies that were used to compare our photometry, listing the 2MASX identification in column (1), the Galactic coordinates in columns (2) and (3) from the 2MASX catalogue, the 2MASX and *WISE* classification types in columns (4) and (5), the heliocentric radial velocity in column (6), and other literature references taken from the NASA Extragalactic Database (NED)[4] in column (7). For the classification, we used G for a galaxy and IrS for an IR source, taken from 2MASX and WISE surveys. The radial velocities were mainly obtained from the H I survey (Staveley-Smith et al. 2016). Following Schröder et al. (2019a), all these sources have flag=1 or 'obvious galaxy' with the exception of 2MASX J12164837−6103579 with flag=2 or 'galaxy'.

For the 164 2MASX extended objects that are not extragalactic, we searched for the closest object in a circle of 1 arcmin radius using the SIMBAD data base.[5] We also identified these sources with different surveys at other frequencies. Table B2 shows interesting information of the 164 2MASX extended objects, listing the 2MASX identification in column (1), the Galactic coordinates in columns (2) and (3) from the 2MASX catalogue, the SIMBAD ID of the closest source in the database and the corresponding literature references in columns (4) and (5), and the object description in column (6). In general, we took the object description from the SIMBAD data base, and for the cases without previous descriptions (about 16 per cent of the total) we added our comments after the visual inspection. The source 2MASX J13464910−6024299 is the known CenB, a well-studied radio source, and we included only 5 of the 59 available references in the table. The sources 2MASX J13462058−6247497, J16103869−4905591, J16152012−4913215, and J17134463−3705111 have the Schröder et al. (2019a) flags 8p?, 9, 9p, and 8p?, respectively, in agreement with our description. Fig. B1 shows the VVV colour composed images of some examples of these 2MASX objects, such as H II regions (1. 12100188−6250004 and 3. 12530717−6350331), YSO candidates (2. 12411836−6144427, 5. 16062307−5043275, and 8. 16574897−4034050), IR sources (6. 16170265−5047083 and 7. 16221035−5006168), and emission-line stars (4. 13462058−6247597).

[4]The NASA/IPAC Extragalactic Database (NED) is operated by the Jet Propulsion Laboratory, California Institute of Technology, under contract with the National Aeronautics and Space Administration.

[5]This research has made use of the SIMBAD data base, operated at CDS, Strasbourg, France.

Table B1. 2MASX extragalactic sources.

2MASX ID	*l* (deg)	*b* (deg)	2MASX type	*WISE* type	Radial velocity ($km\,s^{-1}$)	References
J11494881−6400073	296.2408	− 1.9336	IrS	G	2119 ± 7	1, 2, 3, 4, 5, 6, 7, 14, 16
J11523245−5950248	295.5898	2.1891	G	G	5400 ± 15	8, 14, 16
J11565971−6019148	296.2382	1.8419	G	G	–	8
J12092077−6229125	298.0924	− 0.0111	IrS	IrS	1449 ± 14	2, 4, 14, 16
J12120649−6045031	298.1435	1.7548	IrS	IrS	–	14
J12153835−6102448	298.6112	1.5253	G	G	–	14
J12164837−6103579	298.7541	1.5244	G	G	–	14
J12190068−6024475	298.9365	2.2067	G	G	–	–
J12280968−6054558	300.1055	1.8283	G	IrS	5011 ± 51	2, 14, 16
J12294880−6107045	300.3227	1.6442	G	IrS	5391 ± 319	2, 4, 14, 16
J13281021−6022580	307.4590	2.1650	IrS	IrS	–	9, 14
J13440358−6019350	309.4047	1.8822	IrS	IrS	–	7, 9, 10, 14
J13464910−6024299	309.7214	1.7315	G	G	3872 ± 20	6, 9, 11, 14, 15
J13471848−6034133	309.7457	1.5600	IrS	IrS	–	9, 12, 13, 14
J13502487−6005380	310.2259	1.9398	G	IrS	–	14
J14062119−6025446	312.0511	1.1096	G	IrS	–	2, 8, 13, 14
J14155209−5855348	313.6519	2.1768	G	IrS	5399 ± 4	2, 4, 8, 14
J14391130−5742293	316.9480	2.2014	G	IrS	–	6, 8, 14
J15232096−5915266	321.2764	− 1.9076	IrS	IrS	–	14
J15395406−5737113	323.9908	− 1.8069	G	G	–	8, 14
J16174633−4751584	334.6618	1.8824	G	G	–	8, 14

Notes: References: 1: Kourkchi & Tully (2017), 2: Said et al. (2016), 3: Courtois & Tully (2015), 4: Williams et al. (2014), 5: Courtois et al. (2009), 6: Paturel et al. (2003), 7: Vauglin et al. (2002), 8: Karachentseva et al. (2010), 9: Schröder et al. (2007), Rousseau et al. (2000), 11: Jarrett (2004), 12: Nagayama et al. (2004), 10: Mitronova et al. (2004), 14: Schröder et al. (2019a), 15: West & Tarenghi (1989), 16: Staveley-Smith et al. (2016)

Table B2. 2MASX Galactic sources.

2MASX ID	*l* (deg)	*b* (deg)	SIMBAD ID	References	Description
J11402953−6327520	295.1064	− 1.6758	La Serena 003	1	Possible (open) star cluster
J11450474−6317459	295.5581	− 1.3783	La Serena 009	1	Possible (open) star cluster
J11520923−6153348	296.0102	0.1794	IRAS 11496−6136	2	Carbon star
J11535055−6420218	296.7457	− 2.1616	VVV CL007	3	Cluster of stars
J11585505−6337470	297.1394	− 1.3502	G297.1390−01.3510	4	IR source
J12005699−6304097	297.2516	− 0.7558	La Serena 017	1	Possible (open) star cluster
J12090125−6315596	298.1830	− 0.7866	ESO 95-1	5	H II (ionized) region
J12095662−6249224	298.2143	− 0.3319	Caswell CH3OH 298.22−00.33	6	Maser
J12100013−6250474	298.2247	− 0.3541	–	–	Star
J12100188−6250004	298.2259	− 0.3407	G298.2−00.3	7	H II (ionized) region
J12114684−6146291	298.2609	0.7368	VVV CL010	3	Cluster of stars
J12152350−6301156	298.8570	− 0.4348	[HLB98] SEST 54	8	Maser
J12152500−6301207	298.8600	− 0.4358	G298.8591−00.4372	14	YSO
J12204537−6310426	299.4790	− 0.5126	–	–	Star with a bright nearby star
J12294170−6213085	300.4012	0.5458	IRAS 12268−6156	5	Dense core
J12300399−6256387	300.5045	− 0.1731	G300.5047−00.1745	4	H II (ionized) region
J1232497−6135310	300.7200	1.1998	[MHL2007] G300.7221+01.2007	14	YSO
J12344923−6139290	300.9607	1.1501	–	–	Star
J12345078−6139070	300.9633	1.1564	WRAY 16−118	9	PN
J12345259−6140190	300.9682	1.1366	VVV CL015	3	Cluster of stars
J12345752−6139401	300.9772	1.1480	G300.9785+01.1459	4	IR source
J12350355−6141451	300.9913	1.1141	VVV CL016	3	Open (Galactic) cluster
J12360541−6150347	301.1221	0.9748	–	–	Star
J12411836−6144427	301.7329	1.1030	G301.7319+01.1030	14	YSO candidate
J12415682−6204187	301.8208	0.7794	G301821+007850	10	Bubble
J12433200−6255130	302.0325	− 0.0624	IRAS 12405−6238	5	H II (ionized) region
J12501909−6134572	302.7987	1.2889	DBS2003 80	11	Open (Galactic) cluster
J12502553−6135223	302.8115	1.2819	DBS2003 80	11	Open (Galactic) cluster
J12530717−6350331	303.1173	− 0.9714	IRAS 12500−6334	5	H II (ionized) region
J12545111−6102526	303.3453	1.8211	IRAS 12518−6046	12	Far-IR source
J12552193−6104510	303.4070	1.7873	–	–	Nebula
J13083302−6214482	304.9227	0.5588	DBS2003 82	11	Cluster of stars
J13084090−6215161	304.9375	0.5501	HTU2013 2	13	Dense core
J13110865−6234415	305.1986	0.2068	G305.197+0.206	13	H II (ionized) region
J13111431−6245005	305.1962	0.0345	DBS2003 83	11	Cluster of stars
J13111621−6245505	305.1988	0.0204	DBS2003 84	11	Cluster of stars
J13121738−6242198	305.3198	0.0695	DBS2003 132	11	Cluster of stars
J13122717−6233047	305.3510	0.2217	G305.348+0.223	13	H II (ionized) region
J13142096−6244230	305.5520	0.0154	IRAS 13111−6228	5	H II (ionized) region
J13142635−6244309	305.5621	0.0123	G305.561+0.013	14	YSO candidate
J13270813−6203201	307.1010	0.5269	DZOA 4638−16	15	IR source
J13324267−6026541	308.0094	2.0147	G308.0023+02.0190	14	YSO Candidate
J13405761−6145447	308.7543	0.5482	DZOA 4648−07	15	IR source
J13455154−6009067	309.6594	2.0071	–	–	Star
J13462058−6247597	309.1589	− 0.5939	IRAS 13428-6232	17	Emission-line star
J13463702−6239303	309.2196	− 0.4622	AGAL G309.221−00.462	18	Submillimetric source
J13503488−6140199	309.8877	0.3982	DZOA 4655−12	15	YSO
J13510266−6130150	309.9796	0.5493	IRAS 13475−6115	12	Star
J13515956−6115394	310.1462	0.7597	Caswell OH 310.146+00.760	6	Maser
J14020791−6148249	311.1783	− 0.0723	[MHL2007] G311.1794−00.0720	14	YSO candidate
J14023620−6105450	311.4253	0.5969	DZOA 4664−05	15	IR source
J14023845−6118190	311.3727	0.3941	–	–	Faint star with bright nearby star
J14084243−6110419	312.1084	0.3092	AGAL G312.108+00.309	18	Submillimetric source
J14143959−6222433	312.4121	− 1.0486	IRAS 14109−6208	12	Far-IR source ($\lambda >= 30\ \mu$m)
J14242344−6205208	313.5772	− 1.1540	AGAL G313.576−01.154	18	YSO
J14245658−6144520	313.7582	− 0.8574	AKARI-IRC-V1 J1424563−614450	19	Star
J14275344−5844595	315.1742	1.8103	–	–	Star with a bright nearby star
J14420173−6030091	316.1402	− 0.4984	BNM96 316.139−0.503	5	H II (ionized) region
J14450462−5949094	316.7704	− 0.0363	SMN83 G316.8−0.1 1	20	Part of a cloud
J14450514−5949050	316.7719	− 0.0357	VGO2007 14416−5937 B	21	IR source
J14452278−5949415	316.8011	− 0.0605	WBB2001 41	22	IR source
J14592915−5820102	319.0892	0.4604	IRAS 14556−5808	5	H II (ionized) region
J14593166−5749002	319.3392	0.9158	IRAS 14557−5737	5	H II (ionized) region

Table B2 – *continued*

2MASX ID	*l* (deg)	*b* (deg)	SIMBAD ID	References	Description
J15002412−5924522	318.6831	−0.5455	–	–	No object detected
J15003503−5858101	318.9150	−0.1650	WBB2001 43	22	IR source
J15031365−5904294	319.1630	−0.4206	IRAS 14593−5852	5	H II (ionized) region
J15034121−5835075	319.4522	−0.0213	VVV CL044	3	Cluster of stars
J15051680−5731176	320.1555	0.8043	WRAY 16−160	9	PN
J15160510−5811445	321.0508	−0.5063	AGAL G321.054−00.507	18	Submillimetric source
J15183778−5638505	322.1607	0.6262	MSX5C G322.1587+00.6262	4	IR source
J15202255−5627119	322.4679	0.6611	IRAS 15165−5616	23	Star
J15325265−5556106	324.1995	0.1206	IRAS 15290−5546	5	H II (ionized) region
J15370333−5500156	325.2236	0.5332	–	–	Star with a bright nearby star
J15373472−5534467	324.9446	0.0246	–	–	Star
J15421778−5358308	326.4482	0.9056	IRAS 15384−5348	5	H II (ionized) region
J15433657−5357522	326.6084	0.7972	VVV CL055	3	Cluster of stars
J15444145−5405599	326.6518	0.5931	[DBS2003] 95	5	H II (ionized) region
J15450053−5402059	326.7284	0.6160	[RA2006b] IRS 2	24	NIR source ($\lambda < 10\ \mu$m)
J15455314−5430042	326.5440	0.1691	AGAL G326.544+00.169	18	Submillimetric source
J15462068−5410535	326.7932	0.3802	IRAS 15425−5401	23	Outflow candidate
J15491623−5425461	326.9747	−0.0788	IRAS 15453−5416	23	Star
J15500315−5403503	327.2922	0.1353	–	–	Star
J15530050−5434515	327.3015	−0.5377	MSX6C G327.3017−00.5382	4	IR source
J15530199−5435425	327.2953	−0.5509	AGAL G327.301−00.552	18	YSO
J15530579−5435206	327.3063	−0.5520	GAL 327.3−00.5	25	H II (ionized) region
J15540626−5311391	328.3071	0.4310	GAL 328.31+00.45	26	H II (ionized) region
J15540750−5323442	328.1812	0.2737	SDC G328.178+0.285	27	Dark cloud (nebula)
J15560795−5419395	327.8128	−0.6322	MMB G327.808−00.634	28	Maser
J15575303−5402134	328.1960	−0.5751	IRAS 15539−5353	5	H II (ionized) region
J15581658−5207370	329.4774	0.8426	[MHL2007] G329.4761+00.8414 2	14	YSO candidate
J15593814−5345369	328.5721	−0.5321	GUM 50	29	H II (ionized) region
J15594129−5344479	328.5868	−0.5268	TYC 8697−1749-1	30	Star
J16005582−5236231	329.4725	0.2150	IRAS 15570−5227	5	H II (ionized) region
J16011315−5234360	329.5252	0.2087	MMB G329.526+00.216	28	Maser
J16015300−5356196	328.7059	−0.8840	IRAS 15579−5347	12	Far-IR source ($\lambda >= 30\ \mu$m)
J16055177−5048136	331.2379	1.0617	AGAL G331.239+01.059	31	Submillimetric source
J16062307−5043275	331.3524	1.0657	2MASS J16062311−5043276	14	YSO candidate
J16062662−5043302	331.3589	1.0589	[CPA2006] S59	32	Bubble
J16075456−4918476	332.4815	1.9473	–	–	No object detected
J16103869−4905591	332.9552	1.8021	IRAS 16069−4858	5	H II (ionized) region
J16121310−5202389	331.1301	−0.5220	IRAS 16083−5154	5	H II (ionized) region
J16124234−5145015	331.3859	−0.3593	VVV CL063	3	Cluster of stars
J16150065−4950392	332.9614	0.7739	[DBS2003] 102	33	Open (Galactic) cluster
J16151362−4948505	333.0074	0.7717	SSTGLMC G333.0075+00.7709	34	AGB star candidate
J16151868−4948535	333.0167	0.7617	[GGB2012] G333.0162+00.7615	35	Outflow candidate
J16152012−4913215	333.4291	1.1868	PN Pe 1−5	36	PN
J16164238−5117132	332.1561	−0.4532	GAL 332.15−00.45	26	H II (ionized) region
J16170265−5047083	332.5428	−0.1297	2MASS J16170288−5047051	37	NIR source ($\lambda < 10\ \mu$m)
J16185735−5023591	333.0294	−0.0650	MSX6C G333.0299−00.0645	38	H II (ionized) region
J16190102−5020341	333.0763	−0.0312	–	–	Star with bright nearby stars
J16192228−5009150	333.2489	0.0637	IRAS 16156−5002	5	H II (ionized) region
J16195698−5045452	332.8874	−0.4343	–	–	Star with bright nearby star
J16200971−4936012	333.7284	0.3687	PN G333.7+00.3	4	Possible PN
J16201048−5053291	332.8221	−0.5509	2MASS J16201045−5053286	14	YSO candidate
J16203332−5040423	333.0148	−0.4419	MSX5C G333.0149−00.4431	4	IR source
J16205968−5035141	333.1284	−0.4263	[MHL2007] G333.1306−00.4275 3	14	YSO candidate
J16210034−5036143	333.1179	−0.4393	[MKN2004] MMS 40	50	Millimetric radio source
J16210050−5035089	333.1310	−0.4268	[MHL2007] G333.1306−00.4275 1	14	YSO candidate
J16213188−5025042	333.3085	−0.3664	AGAL G333.308−00.366	18	YSO
J16220862−5005405	333.6062	−0.2070	–	–	IR source
J16221035−5006168	333.6023	−0.2174	MSX5C G333.6044−00.2165	4	IR source
J16225317−5048489	333.1801	−0.7981	CD-50 10459	39	Emission-line star
J16265564−4909491	334.8132	−0.1072	MSX6C G334.8128−00.1059	40	IR source
J16395987−4851524	336.4891	−1.4760	–	–	YSO
J16405900−4707080	337.9057	−0.4423	2MASS J16405819−4706319	40	AGB star candidate
J16410569−4707383	337.9119	−0.4621	[PLW2012] G337.909−00.462-039.2	41	Dense core

Table B2 – *continued*

2MASX ID	*l* (deg)	*b* (deg)	SIMBAD ID	References	Description
J16410805−4706463	337.9272	− 0.4575	[MHL2007] G337.9266−00.4588 1	14	YSO candidate
J16410990−4708074	337.9138	− 0.4764	EGO G337.91−0.48	42	Outflow candidate
J16431592−4605409	338.9342	− 0.0620	–	–	IR source
J16521117−4703067	339.1934	− 1.8506	2MASS-GC03	43	Globular cluster
J16534645−4316088	342.2984	0.3288	VVV CL089	3	Open (Galactic) cluster
J16541460−4517282	340.7828	− 1.0124	AGAL G340.784−01.016	31	Submillimetric source
J16541621−4519002	340.7659	− 1.0322	–	–	Star
J16541764−4517122	340.7918	− 1.0165	RCW 110B	51	H II (ionized) region
J16560261−4304439	342.7066	0.1268	[GBM2006] 16524−4300A	44	Radio source
J16563986−4013290	345.0065	1.8214	[MHL2007] G345.0052+01.8209 1	14	YSO candidate
J16564527−4014280	345.0044	1.7977	IRAS 16533−4009	4	H II (ionized) region
J16574897−4034050	344.8746	1.4360	[MHL2007] G344.8746+01.4347 1	14	YSO candidate
J16592078−4232376	343.5024	− 0.0142	MSX6C G343.5024−00.0145	4	IR source
J16593051−4010419	345.3804	1.4247	[CAB2011] G345.37+1.42	45	Millimetric radio source
J16593668−4003251	345.4880	1.4842	[GGR2014] 1	46	Millimetric radio source
J16593754−4005271	345.4630	1.4611	[MHL2007] G345.4640+01.4581 1	14	YSO candidate
J16594225−4003451	345.4946	1.4668	IRAS 16562−3959	47	Star-forming region
J16594625−4004141	345.4961	1.4518	–	–	Nebula
J17003381−4034210	345.1940	1.0234	–	–	Star
J17003600−4033300	345.2095	1.0266	[DBS2003] 113	33	Cluster of stars
J17003811−4032379	345.2249	1.0303	MSX6C G345.2244+01.0304	4	IR source
J17041301−4220009	344.2194	− 0.5953	2MASX J17041301−4220009	43	Cluster of stars
J17042084−4044456	345.4955	0.3495	[MCM2005b] 89	33	Cluster of stars
J17042791−4046186	345.4885	0.3160	MSX6C G345.4881+00.3148	4	H II (ionized) region
J17043294−4039237	345.5898	0.3734	AGAL G345.589+00.372	48	YSO
J17051332−4101242	345.3751	0.0498	–	–	Stars
J17093532−4135589	345.4062	− 0.9519	[DBS2003] 116	33	Cluster of stars
J17134463−3706111	349.5094	1.0554	NGC 6302	36	PN
J17182142−3919134	348.2307	− 0.9700	–	–	IR source
J17182340−3918444	348.2410	− 0.9706	[TPR2014] IRAS 17149 B3	49	Star in nebula
J17182590−3919264	348.2361	− 0.9839	MSX5C G348.2362−00.9804	52	IR source
J17182961−3919024	348.2484	− 0.9899	[BBC2006] IRAS 17149−3916 Clump 4	53	Dense core
J17191552−3904324	348.5314	− 0.9724	[BNM96] 348.534−0.973	5	H II (ionized) region
J17192058−3903543	348.5494	− 0.9797	[GMB2007b] 17158−3901 C	50	Millimetric radio source
J17195582−3900424	348.6585	− 1.0427	[MHL2007] G348.6600−01.0446 1	14	YSO candidate
J17200331−3858039	348.7085	− 1.0374	–	–	Star
J17200631−3858379	348.7063	− 1.0507	–	–	Star in nebula
J17200691−3859539	348.6901	− 1.0644	–	–	Stars

Notes: References: 1: Barbá et al. (2015), 2: Kwok, Volk & Bidelman (1997), 3: Borissova et al. (2011), 4: Egan et al. (2003), 5: Bronfman, Nyman & May (1996), 6: Caswell, Haynes & Goss (1977), 7: Goss & Shaver (1970), 8: Harju et al. (1998), 9: Wray (1966), 10: Simpson et al. (2012), 11: Dutra et al. (2003), 12: Helou & Walker (1988), 13: Hindson et al. (2013), 14: Mottram et al. (2007), 15: Schröder et al. (2007), 16: Suárez et al. (2006), 17: Urquhart et al. (2014), 18: Caratti o Garatti et al. (2015), 19: Shaver et al. (1983), 20: Vig et al. (2007), 21:Walsh et al. (2001), 22: Ishihara et al. (2010), 23: Roman-Lopes & Abraham (2006), 24: Giveon et al. (2002), 25: Jones & Dickey (2012), 26: Peretto & Fuller (2009), 27: Caswell et al. (2010), 28: Gum (1955), 29: Pinheiro, Copetti & Oliveira (2010), 30: Contreras et al. (2013), 31: Churchwell et al. (2006), 32: Morales et al. (2013), 33: Robitaille et al. (2008), 34: Guzmán et al. (2012), 35: Frew, Bojičić & Parker (2013), 36: Cutri et al. (2003), 37: Yu & Xu (2016), 38: Stephenson & Sanduleak (1971), 39: Robitaille et al. (2007), 40: Purcell et al. (2012), 41: Cyganowski et al. (2008), 42: Kharchenko et al. (2013), 43: Garay et al. (2006), 44: Culverhouse et al. (2011), 45: Guzmán et al. (2014), 46: Araya et al. (2005), 47: Urquhart et al. (2018), 48: Tapia et al. (2014), 49: Garay et al. (2007), 50: Mookerjea et al. (2004), 51: Kuchar & Clark (1997), 52: Egan et al. (2001), 53: Beltrán et al. (2006)

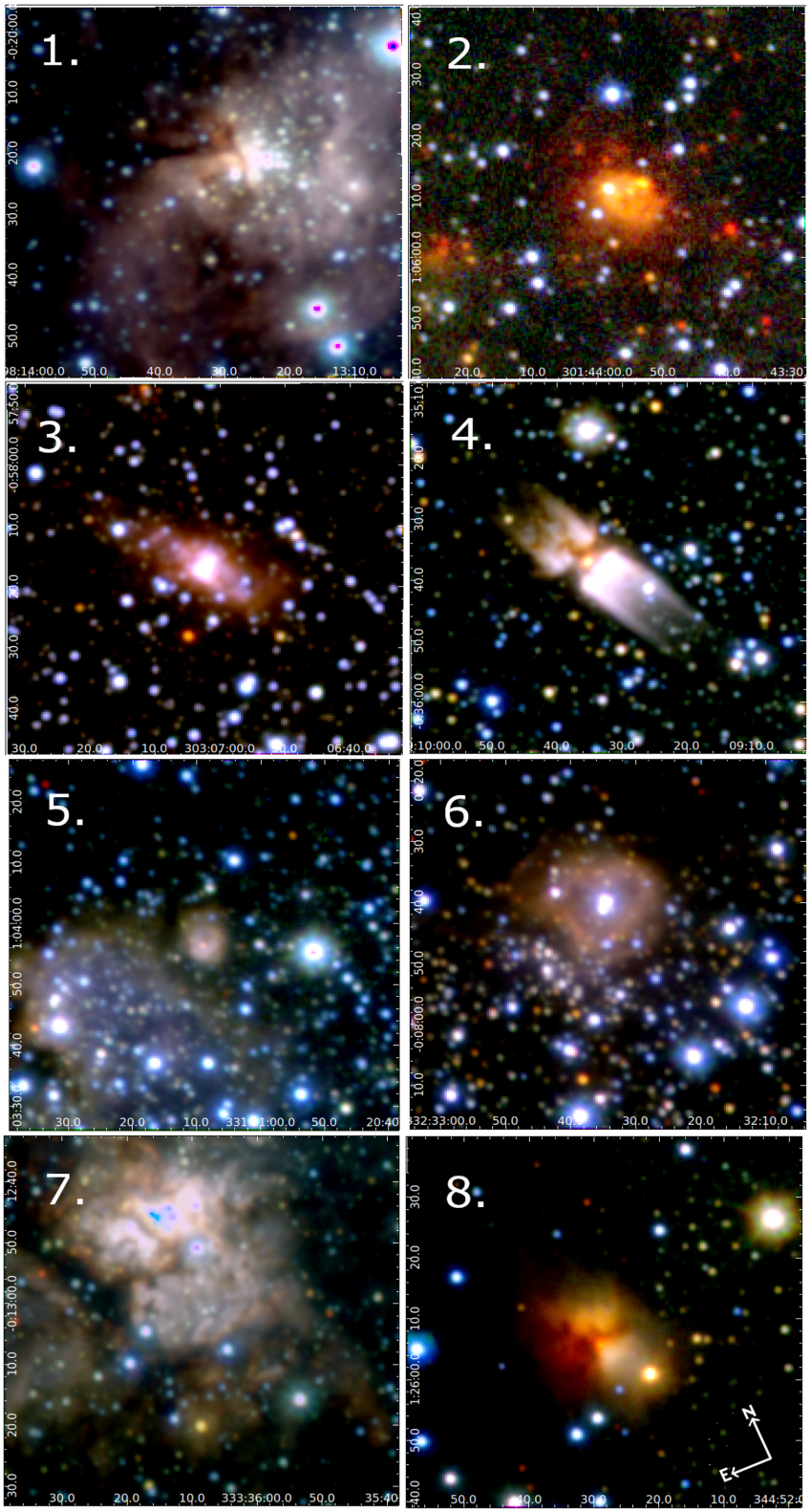

Figure B1. The VVV colour composed images of some Galactic examples of the 2MASS extended sources. The panels show the sources: 1. J12100188−6250004, 2. J12411836−6144427, 3. J12530717−6350331, 4. J13462058−6247597, 5. J16062307−5043275, 6. J16170265−5047083, 7. J16221035−5006168, and 8. J16574897−4034050.

This paper has been typeset from a TEX/LATEX file prepared by the author.